CRinc

THE UNIVERSITY of KANSAS CENTER FOR RESEARCH, INC.
2291 Irving Hill Drive-Campus West Lawrence, Kansas 66045

SCATTERING MODELS IN THE MICROWAVE REGIME

Final Report

October 1984

Prepared for NASA Goddard Space Flight Center
CONTRACT NAG5-268

Principle Investigator: Adrian K. Fung

I. Introduction

The goal of the first year effort was to calculate scattering from an inhomogeneous layer with irregular boundaries to model natural terrains such as a layer of vegetation or sea ice. The inhomogeneities were modeled by spherical or disc-shaped discrete scatterers which were small compared with the incident wavelength and were in the far field of one another. It was found that the cross-polarized scattering was dominated by multiple scattering effects and was sensitive to the orientations and distributions of the scatterers. This model has been applied to interpret measurements from vegetation, snow and sea ice.

The goal of the second year was to extend the scattering model developed in the first year to handle disc-shaped scatterers which are comparable to the incident wavelength and to use the scattering model to investigate the relative merits between active versus passive sensing of soil moisture over vegetated terrain. Results indicate that scattering measurements are more sensitive to soil moisture changes than emission measurements. This is because while both types of measurements lose sensitivity to soil moisture because of the vegetation layer, the loss is greater for passive than active measurements

II. Work Accomplished

The results of the investigation during the first year have been documented and published. Details are given in three papers appended to this report as Appendices A, B, and C.

Part of the results of the second year effort has also been published. This part appears in Appendix D. Other results of the second year study have been documented for publication. It is appended as Appendix E in this report.

III. Conclusions

Significant progresses have been made in the previous years. We are looking forward to continue our efforts at the University of Texas at Arlington to make further progress in the theoritical modeling area.

APPENDIX A

SCATTERING FROM RANDOMLY ORIENTED SCATTERERS OF ARBITRARY SHAPE IN THE LOW-FREQUENCY LIMIT WITH APPLICATION TO VEGETATION

SCATTERING FROM RANDOMLY ORIENTED SCATTERERS OF ARBITRARY SHAPE IN THE LOW-FREQUENCY LIMIT WITH APPLICATION TO VEGETATION

M.A. Karam and A.K. Fung
Remote Sensing Laboratory
University of Kansas Center for Research, Inc.
Lawrence, Kansas, USA 66045

Abstract

A general theory of intensity scattering from small particles of arbitrary shape has been developed based on the radiative transfer theory. Upon permitting the particles to orient in accordance with any prescribed distribution, scattering models can be derived. By making an appropriate choice of the particle size, the scattering model may be used to estimate scattering from media such as snow, vegetation and sea ice. For the purpose of illustration only comparisons with measurements from a vegetated medium are shown. The difference in scattering between elliptic- and circular-shaped leaves is demonstrated. In the low-frequency limit, the major factors on backscattering from vegetation are found to be the depth of the vegetation layer and the orientation distribution of the leaves. The shape of the leaf is of secondary importance.

1. Introduction

The scattering from randomly oriented circular discs has been used to model wave scattering from a vegetation canopy.[1-5]

This study deals with scattering from randomly oriented scatterers of arbitrary shape in the low-frequency limit. First, a general representation of the polarizability tensor in the reference frame is obtained in terms of the angles of orientation and the polarizability tensor in the local frame (the principal frame of the scatterer). Then the polarizability tensor is used to calculate the scattering amplitude when the scatterer is illuminated by an incident plane wave. From the scattering amplitude the backscattering cross-section for a layer of randomly oriented scatterers may be computed based on the first-order solution of the equation of transfer.[6] As an illustration, the study is specialized to the case of randomly oriented elliptically shaped leaves to model scattering by a vegetation canopy. Differences in scattering between circular versus elliptic leaves are illustrated.

2. The Polarizability Tensor In The Reference Frame

For a wave incident upon an arbitrarily shaped scatterer with all dimensions small compared with the electromagnetic wavelength, the scattered field due to the presence of the scatterer can be represented by that radiated from an equivalent dipole with moment $\bar{P}$,[7]

$$\bar{P} = \bar{\bar{\alpha}} \cdot \bar{E}_i \tag{1}$$

where $\bar{E}_i$ is the applied field in the absence of the scatterer and $\bar{\bar{\alpha}}$ is the polarizability tensor.

For a scatterer with its principal axes coinciding with the local frame, the polarizability tensor can be written as,

$$\bar{\bar{\alpha}}_\ell = \sum_{i=1}^{3} \alpha'_{ii} \hat{x}'_i \hat{x}'_i \tag{2}$$

where α'_{ii}'s depend on the electric properties and the dimensions of the scatterer,[8] and $\hat{x}'_i$'s (with $\hat{x}'_1=\hat{x}'$, $\hat{x}'_2=\hat{y}'$, $\hat{x}'_3=\hat{z}'$) are the local frame axes related to the reference frames $\hat{x}_i$ through angles of rotation (α,β,γ)[5]

$$\hat{x}'_i = \sum_{m=1}^{3} \lambda_{im} \hat{x}_m \tag{3}$$

where λ_{im}'s are given in Appendix A of Ref. 9.

To transform the polarizability tensor from the local frame to the reference frame we multiply Eq. 2 from both sides by the unit dyadic

$$\bar{\bar{I}} = \sum_{m=1}^{3} \hat{x}_m \hat{x}_m \tag{4}$$

yielding

$$\bar{\bar{\alpha}}_p = \sum_{m=1}^{3} \sum_{n=1}^{3} \alpha_{mn} \hat{x}_m \hat{x}_n \tag{5}$$

where

$$\alpha_{mn} = \sum_{i=1}^{3} \alpha'_{ii} \lambda_{im} \lambda_{in} = \alpha_{nm} \tag{6}$$

From Eq. 6 it is clear that $\bar{\bar{\alpha}}_p$ is the symmetric tensor. The explicit values of $\bar{\bar{\alpha}}_{mn}$'s are given in Appendix A of Ref. 9. In the special case of a sphere[7] we have

$$\alpha'_{ii} \triangleq \alpha_\ell = \frac{3(\epsilon_r^2-1)}{(\epsilon_r^2+2)} V_0 \tag{7}$$

where $\epsilon_r=\epsilon'_r+j\epsilon''_r$ is the relative dielectric constant of the scatterer with respect to that of the host medium; and V_0 is the volume of the scatterer. (Note: there is a 4π difference between values of α'_{ii}'s and those reported in Refs. 7 and 10. This factor depends on how we express the scattered field in terms of α'_{ii}'s.) Substituting Eq. 6 into 5 we obtain

$$\alpha_{mn} = \alpha_\ell \sum_{i=1}^{3} \lambda_{im} \lambda_{in} = \alpha_\ell \delta_{mn} \tag{8}$$

where δ_{mn} is the Kronecker delta.

3. The Scattering Amplitudes In The Reference Frame

For a wave incident upon a randomly oriented scatterer in $\hat{i}$ direction with polarization vectors $\hat{h}^i$ and $\hat{v}^i$ (Fig. 1), the scattering amplitude matrix for the scattered wave in $\hat{s}$ direction with polarization vectors $\hat{h}^s$ and $\hat{v}^s$, is given by[1]

$$\bar{\bar{f}}(\hat{s},\hat{i}) = \frac{k^2}{4\pi} \sum_{p=v,h} \hat{p}^s \hat{p}^s \cdot \bar{\bar{\alpha}}_p \cdot \sum_{q=v,h} \hat{q}^i \hat{q}^i$$

$$\triangleq \sum_{p=v,h} \sum_{q=v,h} f_{pq}(\hat{s},\hat{i}) \hat{p}^s \hat{q}^i \tag{9}$$

where $f_{pq}(\hat{s},\hat{i})$ is the scattering amplitude for the scattered wave in $\hat{s}$ direction with polarization p due to an incident wave in $\hat{i}$ direction with polarization q (p=q=v or h); and k is the wave number of the host medium. The polarization vectors $\hat{v}^i$ and $\hat{h}^i$ are related to the incident direction $\hat{i}$ by

$$\hat{h}^i = \hat{z}\times\hat{i}/|\hat{z}\times\hat{i}| \triangleq \sum_{m=1}^{3} h^i_m \hat{x}_m = (\hat{y}\cos\phi_i - \hat{x}\sin\phi_i)$$

$$\hat{v}^i = \hat{h}^i \times \hat{i} \triangleq \sum_{m=1}^{3} v^i_m \hat{x}_m = \cos\theta_i(\hat{x}\cos\phi_i + \hat{y}\sin\phi_i) - \hat{z}\sin\theta_i \tag{10}$$

where

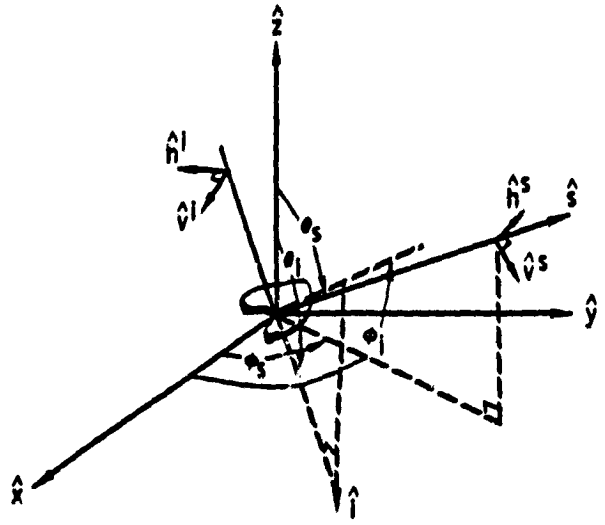

Figure 1. The polarization vectors for the incident and scattered wave.

$$\hat{i} \triangleq \sum_{m=1}^{3} i_m \hat{x}_m = \sin\theta_i(\hat{x}\cos\phi_i+\hat{y}\sin\phi_i)+\hat{z}\cos\theta_i \qquad (11)$$

Similar relations can be written for the scattered wave. Substituting Eq. 5 into 9 we can write $f_{pq}(\hat{s},\hat{i})$ as,

$$f_{pq}(\hat{s},\hat{i}) = \frac{k^2}{4\pi}\sum_{m=1}^{3}\sum_{n=1}^{3} \alpha_{mn} p_m^s q_n^i \qquad (12)$$

To show that Eq. 12 obeys the reciprocity theorem we interchange $\hat{s}$ and $\hat{i}$ in Eq. 12, yielding

$$f_{pq}(\hat{i},\hat{s}) = \frac{k^2}{4\pi}\sum_{m=1}^{3}\sum_{n=1}^{3} \alpha_{mn} q_m^s p_n^i = f_{qp}(\hat{s},\hat{i}) \qquad (13)$$

It is worth noting that α_{mn} depends on α, β, γ and α'_{mn} but is independent of $\hat{s}$ and $\hat{i}$.

4. The Extinction Coefficient For Randomly Oriented Scatterers

For a plane wave propagating in $\hat{i}$ direction defined by $\Omega_i(\theta_i,\phi_i)$ through a collection of randomly oriented scatterers, the total loss per unit length is given by the extinction coefficients as,

$$k_q(\hat{i}) = \sum_{\ell=a,s} k_{\ell q}(\hat{i}) \qquad (14)$$

The subscript a stands for absorption, the subscript s for scattering and the subscript q=v or h represents the polarization of the incident wave.

The scattering coefficients can be written as[2]

$$k_{sq}(\hat{i}) = \sum_{p=v,h}\int_{4\pi} d\Omega_s \langle |f_{pq}(\hat{s},\hat{i})|^2\rangle \qquad (15)$$

where $d\Omega_s$ is the differential solid angle in the direction of the scattered wave $\hat{s}$, and the ensemble average $\langle\rangle$ is taken over the spatial distribution and orientations of the scatterer. The spatial averaging is equivalent to multiplying Eq. 15 by the number density N_0. From Eq. 12 we can write:

$$|f_{pq}(\hat{s},\hat{i})|^2 = \left|\frac{k^2}{4\pi}\right|^2 \sum_{m=1}^{3}\sum_{n=1}^{3}\sum_{\ell=1}^{3}\sum_{j=1}^{3} \alpha_{mn}\alpha^*_{\ell j} q_n^i q_j^i p_m^s p_\ell^s \qquad (16)$$

where * is the complex conjugate symbol. From Eq. 10 and Eqs. (A-11)-(A-17) of Ref. 9 it follows that:

$$\int_{4\pi} p_m^s p_\ell^s \, d\Omega_s = 0 \qquad m \neq \ell \qquad (17)$$

$$\int_{2\pi} \alpha_{mn}\alpha^*_{mj} \, d\alpha = 0 \qquad n \neq j \qquad (18)$$

Substituting Eqs. 17 and 18 in 16 and then 16 into 15 we get

$$k_{sq}(\hat{i}) = N_0\left|\frac{k^2}{4\pi}\right|^2 \cdot \sum_{p=v,h}\int_{4\pi} d\Omega_s \left\langle \sum_{m=1}^{3}\sum_{n=1}^{3} |\overline{\alpha_{mn}}|^2 (q_n^i)^2 (p_m^s)^2 \right\rangle \qquad (19)$$

where $|\overline{\alpha_{mn}}|^2$ is the value of $|\alpha_{mn}|^2$ after integration with respect to α over $(0,2\pi)$. After integrating Eq. 19 with respect to $d\Omega_s$ and summing over n and scattered polarization we can write the scattering coefficient as:

$$k_{sv}(\hat{i}) = \frac{N_0 k^4}{6\pi}\left\langle \left(\sum_{m=1}^{3} |\overline{\alpha_{m1}}|^2\right)\cos^2\theta_i + \left(\sum |\overline{\alpha_{m3}}|^2\right)\sin^2\theta_i \right\rangle \qquad (20)$$

$$k_{sh}(\hat{i}) = \frac{N_0 k^4}{6\pi}\left\langle \left(\sum_{m=1}^{3} |\overline{\alpha_{m2}}|^2\right)\right\rangle \qquad (21)$$

Substituting Eqs. (A-12)-(A-17) into (A-19) of Ref. 9 and then substituting the result (with i=m and j=n) into Eqs. 20 and 21 we can write the scattering coefficient in terms of β, γ and α'_{ij} as:

$$\begin{aligned} k_{sv}(\hat{i}) = \frac{N_0 k^4}{12\pi}\Big\langle & \Big\{\cos^2\beta|\alpha'_{11}|^2 \\ & +(\sin^2\beta+\cos^2\gamma\cos^2\beta)|\alpha'_{22}|^2 \\ & +(\sin^2\beta+\sin^2\gamma\cos^2\beta)|\alpha'_{33}|^2\Big\}\cos^2\theta_i \\ & +2\Big\{\sin^2\beta|\alpha'_{11}|^2+\sin^2\gamma\cos^2\beta|\alpha'_{22}|^2 \\ & +\cos^2\gamma\cos^2\beta|\alpha'_{33}|^2\Big\}\sin^2\theta_i\Big\rangle \end{aligned} \qquad (22)$$

$$\begin{aligned} k_{sh}(\hat{i}) = \frac{N_0 k^4}{12\pi}\Big\langle & \cos^2\beta|\alpha'_{11}|^2+(\sin^2\beta+\cos^2\gamma\cos^2\beta)|\alpha'_{22}|^2 \\ & +(\sin^2\beta+\sin^2\gamma\cos^2\beta)|\alpha'_{33}|^2\Big\rangle \end{aligned} \qquad (23)$$

In Eqs. 22 and 23 the ensemble average $\langle\rangle$ is taken over the scatterer orientation with respect to the angles β and γ. Under the assumption that $\alpha'_{11}=\alpha'_{22}$ and $\gamma=0$, Eqs. 22 and 23 reduce to Eqs. (68) and (69) in Ref. 2.

The absorption coefficient, for a unit incident plane wave in $\hat{i}$ direction with polarization $\hat{q}^i$, can be written as[11]

$$\begin{aligned} k_{aq}(\hat{i}) &= N_0 k\varepsilon''_r \left\langle \int_{V_0} (\overline{Q}_q^i\cdot\overline{Q}_q^{*i})\, dV\right\rangle \\ &= N_0 k\varepsilon''_r \langle(\overline{Q}_q^i\cdot\overline{Q}_q^{*i})\rangle V_0 \end{aligned} \qquad (24)$$

where $\overline{Q}_q^i$ is the electric field inside the scatterer, which is related to the induced dipole moment $\overline{p}_q$ through the relation[7]

$$\overline{Q}_q^i = \frac{1}{V_0(\varepsilon_r-1)}\,\overline{p}_q \qquad (25)$$

From Eqs. 1 and 2 we can write $\overline{p}_q$ as

$$\overline{p}_q = \sum_{m=1}^{3} \alpha'_{mm}(\hat{x}'_m\cdot\hat{q}^i)\hat{x}'_m \qquad (26)$$

Upon substituting Eq. 26 into 25, the field inside the scatterer is

$$\bar{Q}_q^i = \frac{1}{V_0(\epsilon_r-1)} \sum_{m=1}^{3} \alpha'_{mm}(\hat{x}'_m\cdot\hat{q}^i)\hat{x}'_m \tag{27}$$

From Eqs. 24 and 27 the absorption coefficient is

$$k_{aq}(\hat{i}) = N_0 k_a \left\langle \sum_{m=1}^{3} |\alpha'_{mm}|^2 \left(\hat{x}'_m\cdot\hat{q}^i\right)^2 \right\rangle$$

$$= N_0 k_a \left\langle \sum_{m=1}^{3} |\alpha'_{mm}|^2 \left(\sum_{n=1}^{3} \lambda_{mn} q_n^i\right)^2 \right\rangle \tag{28}$$

where

$$k_a = \frac{k\epsilon''_r}{V_0|\epsilon_r-1|^2}$$

Substituting Eq. 10 and Eq. (A-2) of Ref. 9 into Eq. 28 and integrating with respect to α over $(0,2\pi)$ we obtain,

$$k_{av}(\hat{i}) = N_0 k_a \left\langle \tfrac{1}{2}\left\{|\alpha'_{11}|^2\cos^2\beta + |\alpha'_{22}|^2(\sin^2\beta\sin^2\gamma+\cos^2\gamma) + |\alpha'_{33}|^2(\sin^2\beta\cos^2\gamma+\sin^2\gamma)\right\}\cos^2\theta_i + \left\{|\alpha'_{11}|^2\sin^2\beta+|\alpha'_{22}|^2\cos^2\beta\sin^2\gamma + |\alpha'_{33}|^2\cos^2\beta\cos^2\gamma\right\}\sin^2\theta_i \right\rangle \tag{29}$$

$$k_{ah}(\hat{i}) = N_0 k_a \left\langle |\alpha'_{11}|^2\cos^2\beta + |\alpha'_{22}|^2(\sin^2\beta\sin^2\gamma+\cos^2\gamma) + |\alpha'_{33}|^2(\sin^2\beta\cos^2\gamma+\sin^2\gamma)\right\rangle \tag{30}$$

For an elliptic scatterer in the low-frequency limit Eqs. 29 and 30 are equal to the extinction coefficient calculated by using the forward scattering theorem.[9]

5. The Backscattering Cross-Section For A Layer Of Randomly Oriented Ellipsoids

For a collection of identical sparsely distributed randomly oriented lossy dielectric ellipsoids embedded in a layer without upper boundary above a half-space the like- and cross-polarized backscattering cross-sections per unit area computed from the first-order solution of the radiative transfer equation are[6]

$$\sigma_{pq}(\hat{i},\hat{i}) = 4\pi\cos\theta_i\left[\left\langle|f_{pq}(\hat{i}_1,-\hat{i})|^2\right\rangle A_{pq} + \left\langle|f_{pq}(-\hat{i},\hat{i})|^2\right\rangle B_{pq}\right] \tag{31}$$

where

$$A_{pq} = \begin{cases} 2r_p(\hat{i})d\sec\theta_i\exp\left(-2k_p(\hat{i})d\sec\theta_i\right) & , p=q \\ \left[\exp\left(-k_q(\hat{i})d\sec\theta_i\right)-\exp\left(-k_p(-\hat{i})d\sec\theta_i\right)\right] \cdot\left[r_p(\hat{i})\exp\left(-k_p(\hat{i})\sec\theta_i d\right) + r_q(\hat{i})\exp\left(-k_q(\hat{i})d\sec\theta_i\right)\right]/\left(k_p(\hat{i})-k_q(\hat{i})\right) & , p\neq q \end{cases}$$

$$B_{pq} = \left[1-\exp\left(-\left\{k_p(\hat{i})+k_q(\hat{i})\right\}d\sec\theta_i\right)\right] \cdot\left[1+r_p(\hat{i})r_q(\hat{i})\exp\left(-\left\{k_p(\hat{i}) + k_q(\hat{i})\right\}d\sec\theta_i\right)\right]/\left(k_p(\hat{i})+k_q(\hat{i})\right) \tag{32}$$

In Eqs. 31 and 32 $\hat{i}_1$ and $-\hat{i}$ are in $(\theta_i,\pi+\phi_i)$ and (θ_i,ϕ_i) directions, respectively; d is the depth of the layer containing the scatterers; $r_p(\hat{i})$ and $r_q(\hat{i})$ are the Fresnel reflectivities for the interface separating the layer and the lower half-space (p=q=v or h). From Eqs. 10, 16, 18 and Eq. (A-19) of Ref. 9 we can write

$$\left\langle|f_{vv}(-\hat{i},\hat{i})|^2\right\rangle = N_0\left|\frac{k^2}{4\pi}\right|^2 \left\langle \cos^4\theta_i|\overline{\alpha_{11}}|^2 + \sin^2 2\theta_i\left(|\overline{\alpha_{13}}|^2 + \tfrac{1}{2}\overline{\mathrm{Re}(\alpha_{11}\alpha_{33}^*)}\right) + \sin^4\theta_i|\overline{\alpha_{33}}|^2\right\rangle \tag{33}$$

$$\left\langle|f_{vv}(\hat{i}_1,-\hat{i})|^2\right\rangle = N_0\left|\frac{k^2}{4\pi}\right|^2 \left\langle \cos^4\theta_i|\overline{\alpha_{11}}|^2+\sin^4\theta_i|\overline{\alpha_{33}}|^2 - \tfrac{1}{2}\sin^2 2\theta_i\overline{\mathrm{Re}(\alpha_{11}\alpha_{33}^*)}\right\rangle \tag{34}$$

$$\left\langle|f_{vh}(-\hat{i},\hat{i})|^2\right\rangle = \left\langle|f_{vh}(\hat{i}_1,-\hat{i})|^2\right\rangle = N_0\left|\frac{k^2}{4\pi}\right|^2 \left\langle\cos^2\theta_i|\overline{\alpha_{12}}|^2+\sin^2\theta_i|\overline{\alpha_{13}}|^2\right\rangle \tag{35}$$

$$\left\langle|f_{hh}(-\hat{i},\hat{i})|^2\right\rangle = \left\langle|f_{hh}(\hat{i}_1,-\hat{i})|^2\right\rangle = N_0\left|\frac{k^2}{4\pi}\right|^2\left\langle|\overline{\alpha_{11}}|^2\right\rangle \tag{36}$$

The explicit forms of Eqs. 33-36 in terms of β and γ as well as α'_{mn} are given in Appendix C of Ref. 9.

For an elliptic scatterer with semi-axes a_i (i=1, 2, 3) the polarizability tensor elements α'_{ii} are[7]

$$\alpha'_{ii} = \frac{V_0(\epsilon_r-1)}{(\epsilon_r-1)A_i+1} \tag{37}$$

where

$$A_i = \frac{1}{2}\left(\prod_{i=1}^{3} a_i\right)\int_0^\infty \frac{dS}{(S+a_i)R(S)} \tag{38}$$

and

$$R(S) = \prod_{i=1}^{3}(S+a_i)^{1/2}$$

In Eq. 37 V_0 is the volume of the scatterer given by

$$V_0 = \frac{4\pi}{3}\prod_{i=1}^{3} a_i \ .$$

The integral A_i in Eq. 38 can be found in Ref. 12. In case of a thin elliptic disc ($a_1>a_2\geq a_3$) which can be used to model a leaf, we can write[12]

$$A_1 = \frac{a_3}{a_1}\frac{\sqrt{1-e^2}\,F(\pi/2,e)-E(\pi/2,e)}{e^2}$$

$$A_2 = \frac{a_3}{a_1}\frac{E(\pi/2,e)-(1-e^2)F(\pi/2,e)}{e^2\left(1-e^2\right)^{1/2}}$$

$$A_3 = 1-\frac{a_3}{a_1}\frac{E(\pi/2,e)}{\left(1-e^2\right)^{1/2}} \tag{39}$$

where $e=\sqrt{1-(a_2/a_1)^2}$. $F(\pi/2,e)$ and $E(\pi/2,e)$ are complete elliptic integrals of the first and second kind, respectively,[13] given by

$$F(\pi/2,e) = \int_0^{\pi/2}\frac{dS}{\sqrt{1-e^2\sin^2 S}}$$

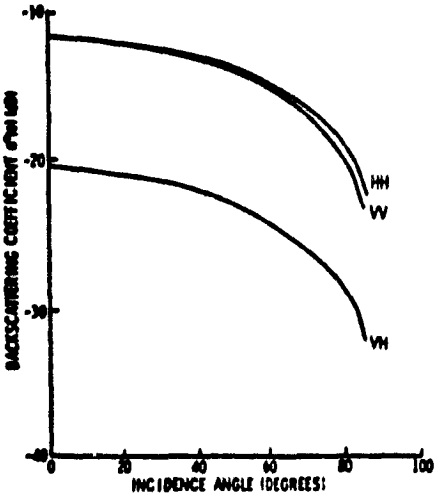

Figure 2. Backscattering from a half-space of randomly oriented elliptic discs [f=1.1 GHz, ϵ_r=30.8+j1.8, a_1=2.8 cm, a_2=0.84 cm, a_3=0.375 mm, $0° \le \beta \le 30°$, $0° \le \gamma \le 90°$, $0° \le \alpha \le 360°$].

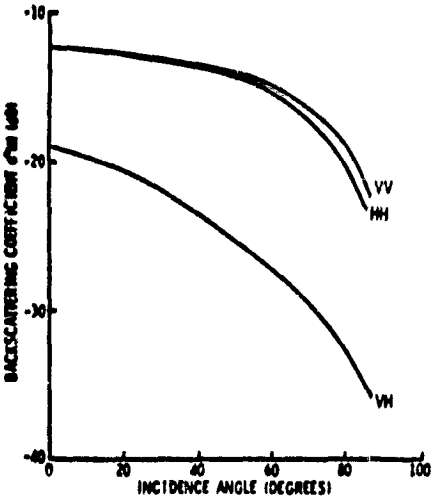

Figure 3. Backscattering from a half-space of randomly oriented elliptic discs [f=1.1 GHz, ϵ_r=30.8+j1.8, a_1=2.8 cm, a_2=0.84 cm, a_3=0.375 mm, $60° \le \beta \le 90°$, $0° \le \gamma \le 90°$, $0° \le \alpha \le 360°$].

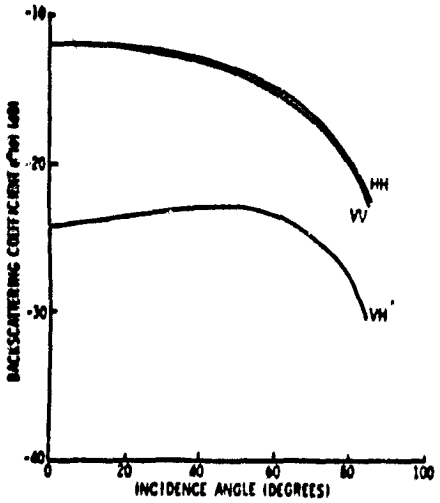

Figure 4. Backscattering from a half-space of randomly oriented elliptic discs [f=1.1 GHz, ϵ_r=30.8+j1.8, a_1=2.8 cm, a_2=0.84 cm, a_3=0.375 mm, $0° \le \beta \le 90°$, $0° \le \gamma \le 30°$, $0° \le \alpha \le 360°$].

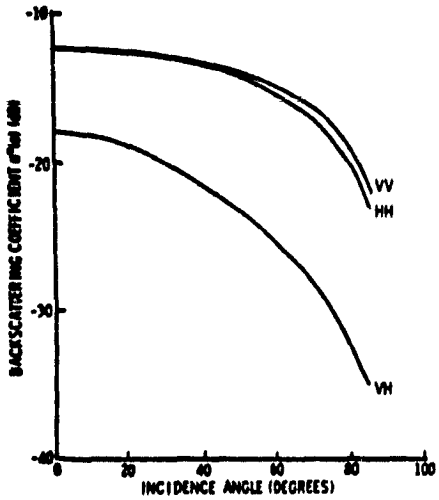

Figure 5. Backscattering from a half-space of randomly oriented elliptic discs [f=1.1 GHz, ϵ_r=30.8+j1.8, a_1=2.8 cm, a_2=0.84 cm, a_3=0.375 mm, $0° \le \beta \le 90°$, $60° \le \gamma \le 90°$, $0° \le \alpha \le 360°$].

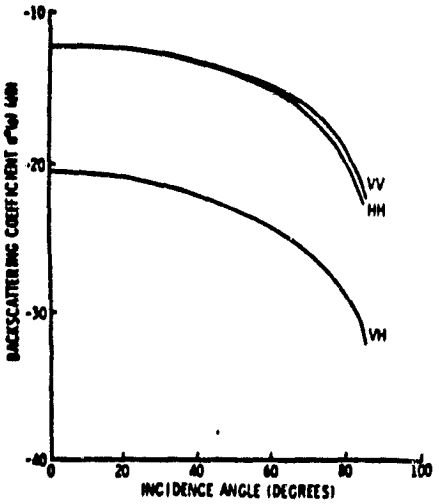

Figure 6. Backscattering from a half-space of randomly oriented elliptic discs [f=1.1 GHz, ϵ_r=30.8+j1.8, a_1=2.8 cm, a_2=0.84 cm, a_3=0.375 mm, $0° \le \beta \le 90°$, $0° \le \gamma \le 90°$, $0° \le \alpha \le 360°$].

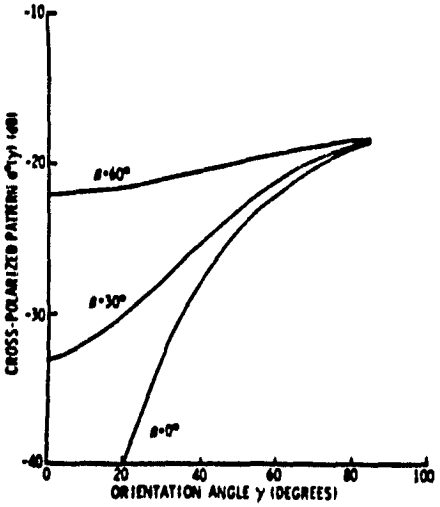

Figure 7. Cross-polarized pattern at normal incidence along circular disc axis [f=1.1 GHz, ϵ_r=30.8+j1.8, $a_1=a_2$=1 cm, a_3=0.872 mm, $0° \le \alpha \le 360°$].

and

$$E(\pi/2,e) = \int_0^{\pi/2} \sqrt{1-e^2\sin^2 S}\, dS$$

When $a_1=a_2$ (oblate spheroid), we can write[12]

$$A_1 = A_2 = \frac{1}{2(m^2-1)}\left\{m^2\left(m^2-1\right)^{-\frac{1}{2}}\sin^{-1}\left[\left(m^2-1\right)^{\frac{1}{2}}/m\right]-1\right\} \tag{40}$$

$$A_3 = \frac{m^2}{(m^2-1)}\left\{1-\frac{1}{\left(m^2-1\right)^{\frac{1}{2}}}\sin^{-1}\left[\left(m^2-1\right)^{\frac{1}{2}}/m\right]\right\} \tag{41}$$

where $m=a_1/a_3$.

In the above a_1, a_2, and a_3 are taken to be parallel to $\hat{x}'$, $\hat{y}'$, $\hat{z}'$ axes, respectively. This means that the orientations of the semi-axes a_1, a_2, a_3 are described by (α,β), (α,β,γ) and (α,β,γ).[9] The tilting of a_1 and a_2 with respect to the local axes are of course controlled by β and γ, respectively.

6. Comparisons Between Circular And Elliptic Discs

In Figs. 2-6 backscattering characteristics from elliptic discs, with dielectric constant based on formula given in Ref. 14, are shown for five different combinations of orientations. In all cases the orientation distributions of the axes not specified below are assumed uniformly distributed over (0°,90°).

(1) The major axis is restricted to small tilt angles, i.e., $0°<\beta<30°$.

(2) The major axis is restricted to large tilt angles, i.e., $60°<\beta<90°$.

(3) The minor axis is restricted to small tilt angles, i.e., $0°<\gamma<30°$.

(4) The minor axis is restricted to large tilt angles, i.e., $60°<\gamma<90°$.

(5) Both axes are uniformly distributed over (0°,90°).

Before discussing the characteristics of the cases shown, note that polarized scattering is usually in agreement with intuition. To understand cross-polarized

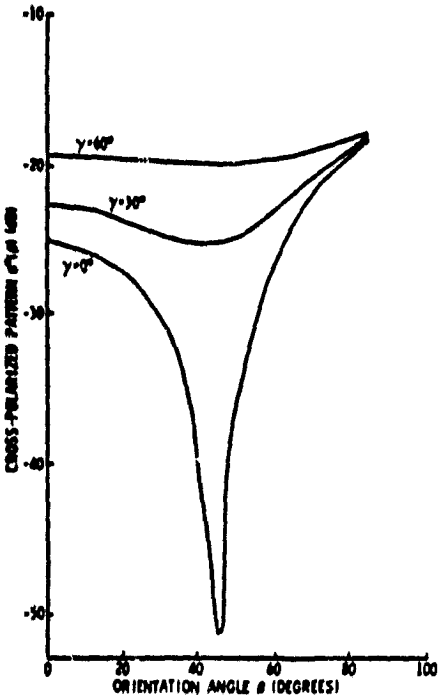

Figure 8a. Cross-polarized pattern at normal incidence along major axis of an elliptic disc [f=1.1 GHz, ϵ_r=30.8+j1.8, a_1=2.8 cm, a_2=0.84 cm, a_3=0.375 mm, $0° \leq \alpha \leq 360°$].

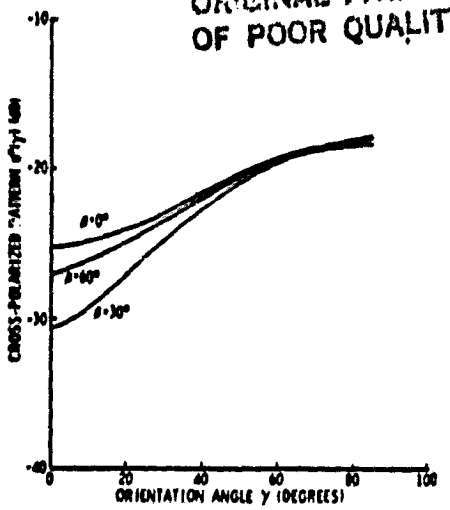

Figure 8b. Cross-polarized pattern at normal incidence along minor axis of an elliptic disc [f=1.1 GHz, ϵ_r=30.8+j1.8, a_1=2.8 cm, a_2=0.84 cm, a_3=0.375 mm, $0° \leq \alpha \leq 360°$].

scattering it should be remembered that the cross-polarized reradiation pattern for small circular discs increases with the increase in the local incidence angle (Fig. 7); while for an elliptic disc of the same volume, this reradiation pattern could have a dip with the increase in the local incidence angle along the plane parallel to the major axis (Fig. 8a). The reradiation pattern parallel to the minor axis shows a minimum at near normal incidence (Fig. 8b).

For case (1) (Fig. 2) the horizontally polarized component at large incidence angles is higher than the vertically polarized component due to the more nearly horizontal disc orientations. The reverse is true in case (2) (Fig. 3) as expected. For the cross-polarized component case (1) shows a slower angular drop off than case (2), since the cross pattern along the major axis or minor axes is close to its maximum at near grazing incidence and assumes smaller values at near normal incidence. In cases (3) and (4) (Figs. 4 and 5) the change in distribution is associated with the minor axis. As expected, the polarized reradiation pattern is more isotropic over the minor axis than the major axis. Hence, this change in distribution produces only small changes in the polarized scattering components. For the cross-polarized component, the smaller tilt angles [case (3)] lead to smaller returns near normal incidence and a slower angular drop off than case (4). This is expected since the cross pattern is at a minimum near the local normal of the disc parallel to the minor axis (Fig. 8b). There are only small differences between cases (4) and (5) for the polarized component for the same reason given for cases (3) and (4). The cross-polarized return of case (5) lies between those of cases (3) and (4) as expected.

In Figs. 9-11, the backscattering curves for circular discs of the same volume as the elliptic discs with major axis equal to the minor axis, the five cases discussed in the previous paragraph reduce to three

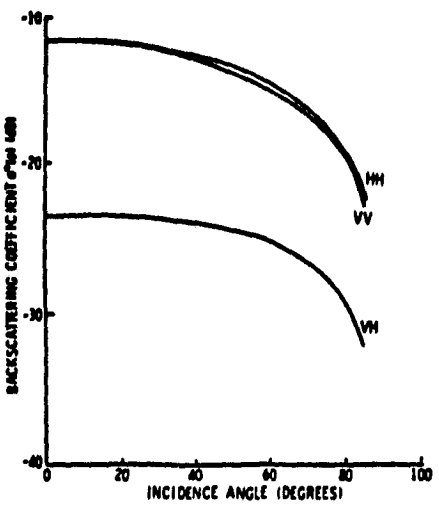

Figure 9. Backscattering from a half-space of randomly oriented circular discs [f=1.1 GHz, ϵ_r=30.8+j1.8, a_1=a_2=1 cm, a_3=0.872 mm, $0° \leq \beta \leq 30°$, $0° \leq \gamma \leq 90°$, $0° \leq \alpha \leq 360°$].

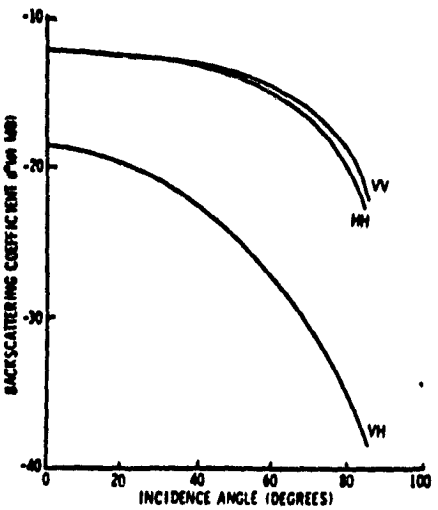

Figure 10. Backscattering from a half-space of randomly oriented circular discs [f=1.1 GHz, ϵ_r=30.8+j1.8, a_1=a_2=1 cm, a_3=0.872 mm, $60° \leq \beta \leq 90°$, $0° \leq \gamma \leq 90°$, $0° \leq \alpha \leq 360°$].

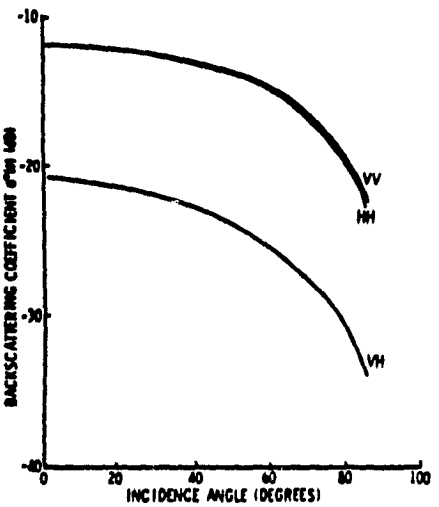

Figure 11. Backscattering from a half-space of randomly oriented circular discs [f=1.1 GHz, ϵ_r=30.8+j1.8, a_1=a_2=1 cm, a_3=0.872 mm, $0° \leq \beta \leq 90°$, $0° \leq \gamma \leq 90°$, $0° \leq \alpha \leq 360°$].

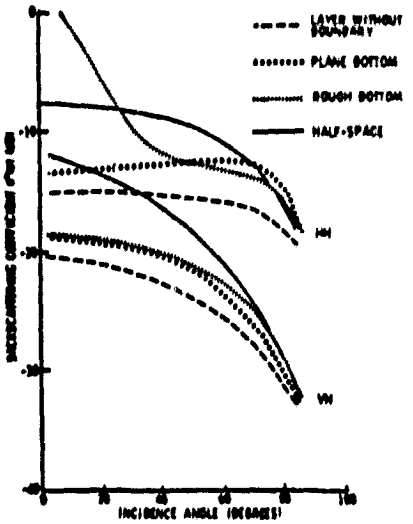

Figure 12. Comparison between backscattering from a half-space, a layer with plane and rough bottom boundaries [f=1.1 GHz, ϵ_r=30.8+j1.8, ϵ_g=10, kσ=1.1, kℓ=8, V_0N_0=0.002, 60°≤β≤90°, 0°≤γ≤90°, 0°≤α≤360°].

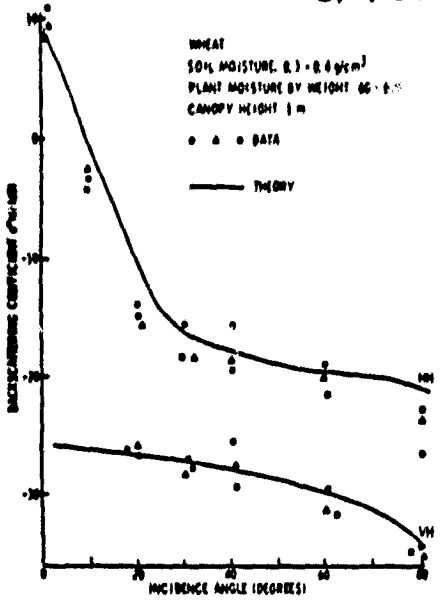

Figure 13. Comparison with measurements of wheat [f=1.5 GHz, ϵ_r=24.5+j1.7, ϵ_g=25, σ=1.1 cm, ℓ=25 cm, a_1=a_2=1.3 cm, a_3=0.02 cm, 0°≤β≤90°, 0°≤γ≤90°, 0°≤α≤360°].

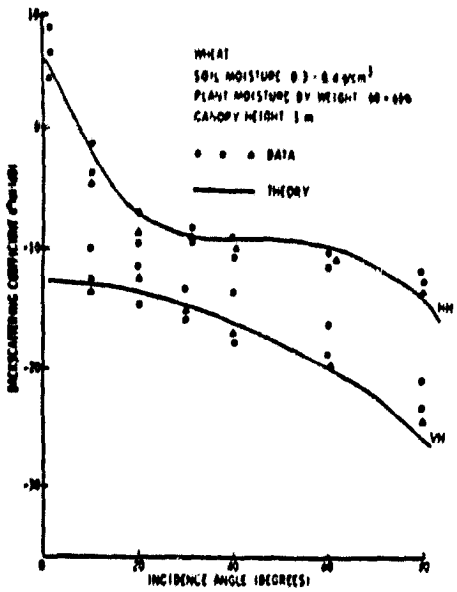

Figure 14. Comparison with measurements of wheat [f=4.25 GHz, ϵ_r=23.5+j4.7, ϵ_g=25, σ=1.1 cm, ℓ=13 cm, a_1=a_2=1.3 cm, a_3=0.02 cm, 0°≤β≤90°, 0°≤γ≤90°, 0°≤α≤360°].

cases. Figs. 9, 10 and 11 are comparable to Figs. 2 or 4, 3 or 5 and 6. The polarized and cross-polarized scattering also follow the general patterns in the corresponding figures for reasons similar to those given in the previous paragraph. Of course, small differences exist in level and trend between the corresponding figures especially for the cross-polarized return (see for example, Figs. 2, 4 and 9). In view of the differences between Figs. 7 and 8a, one would expect much greater difference between elliptic and circular discs. However, due to the assumed random orientation, the difference due to disc shape in this low-frequency case is not as pronounced as one might expect. Instead, significant differences in scattering due to different distributions are very obvious in the cross-polarized return. This implies that the cross-polarized return may serve as one contributing factor for crop identification when significant differences exist between the orientation of leaves and when the leaf distributions in orientation are known for vegetation types to be differentiated.

7. Layer Effect And Comparison With Measurements

In Fig. 12 comparisons are shown between backscattering curves from a vegetated half-space, a vegetated layer without boundaries, a vegetated layer with plane bottom boundary and a vegetated layer with rough bottom boundary. It is seen that scattering from a half-space has a significantly slower angular trend than that of a half-space. For horizontal polarization, the difference between a plane versus a rough layer boundary is small at large angles of incidence for polarized scattering and at small angles of incidence for cross-polarized scattering.

Since the effects dominating the backscattering curves at low frequencies (scatterer small compared with the electromagnetic wavelength) are (1) leaf distribution, (2) layer versus half-space, and (3) surface roughness, in Figs. 13 and 14 we show comparisons with backscatter measurements from wheat[15] using a vegetated layer of circular leaves with a rough bottom boundary. The rough surface scatter model used is the Kirchhoff model under scalar approximation[16] characterized by a standard deviation of surface height σ and surface correlation length ℓ. In both figures, the data trends are fairly flat for the cross-polarized return and peaked near nadir for the polarized return indicating the strong influence of the rough ground interface. Although the leaf of wheat is elliptic, use of circular-shaped leaves with random orientations appears to produce good agreements with data. This means that the effect of leaf shape is indeed not an important factor in low-frequency scattering.

8. Conclusions

In vegetation modeling at low frequencies, the important factors governing the backscattering curves are (1) the roughness of the vegetation-ground interface, (2) the leaf orientation distribution, and (3) the depth of the vegetation layer. It is found that the effect of the leaf shape is not as important a factor although it does have some effect on the level and trend of the angular backscattering curve.

Acknowledgment

This work was supported by the NASA Goddard Space Flight Center under Grant NAG5-268.

References

1. Lang, L.H., "Electromagnetic backscattering from a sparse distribution of lossy dielectric scatterers," *Radio Science*, vol. 16, pp. 15-30, 1981.

2. Tsang, L., M.C. Kubacsi, and J.A. Kong, "Radiative transfer theory for active remote sensing of a layer of small ellipsoidal scatterers," *Radio Science*, vol. 16, no. 3, pp. 321-329, 1981.

3. Lang, L.H. and J. Sidhu, "Electromagnetic backscattering from a layer of vegetation: a discrete approach," *IEEE Trans. Geosci. and Rem. Sens.*, vol. GE-21, no. 1, pp. 62-71, 1983.

4. Lang, R.H., S.S. Seker, and D.M. Le Vine, "Scattering from a random layer of leaves in the physical optics limit," *Digest of IGARSS'82*, Munich, West Germany, June 1-4, 1982.

5. Karam, M.A. and A.K. Fung, "Scattering from randomly oriented circular discs with application to vegetation," RSL TR 485-7, Remote Sensing Laboratory, University of Kansas Center for Research, Inc., Lawrence, Kansas, 1982. (Radio Science, in press)

6. Karam, M.A. and A.K. Fung, "Propagation and scattering in multi-layered random media with rough interfaces," *Electromagnetics*, vol. 2, pp. 239-256, 1982.

7. Van de Hulst, H.C., *Light Scattering by Small Particles*, Dover, New York, pp. 63-84, 1981.

8. Kleinman, R.E., "Low-frequency electromagnetic scattering," in *Electromagnetic Scattering*, edited by P.L.E. Uslegnghi, Academic Press, New York, pp. 1-28, 1978.

9. Karam, M.A. and A.K. Fung, "Scattering from randomly oriented scatterers of arbitrary shape in the low-frequency limit with application to vegetation," RSL TR 592-2, Remote Sensing Laboratory, University of Kansas Center for Research, Inc., Lawrence, Kansas, April 1983.

10. Morse, P.M. and H. Feshbach, *Methods of Theoretical Physics*, McGraw-Hill, Inc., New York, pp. 1886-1891, 1953.

11. Ishimaru, A., *Wave Propagation and Scattering in Random Media*, vol. 1, Academic Press, New York, pp. 14-17, 1978.

12. Osborn, J.A., "Demagnetizing factors of the general ellipsoid," *Physical Review*, vol. 67, pp. 351-357, 1945.

13. Gradshteyn, J.S. and I.M. Ryzhik, *Table of Integrals, Series, and Products*, Academic Press, New York, pp. 904-905, 1980.

14. Fung, A.K. and F.T. Ulaby, "A scatter model for leafy vegetation," *IEEE Trans. Geosci. Electr.*, vol. GE-16, no. 4, pp. 281-286, 1978.

15. Dobson, C., M. Stiles, D. Brunfeldt, T. Metzler, and S. McMeckin, "Data documentation: 1976 MASI-8 and MAS8-18 vegetation experiments," RSL TR 264-15, Remote Sensing Laboratory, University of Kansas Center for Research, Inc., Lawrence, Kansas, 1977.

16. Ulaby, F.T., R.K. Moore, and A.K. Fung, *Microwave Remote Sensing*, vol. 2, Chapter 12, Addison-Wesley, Reading, Massachusetts, 1982.

D2

N85 13363

APPENDIX B

SCATTERING FROM RANDOMLY ORIENTED CIRCULAR DISCS WITH APPLICATION TO VEGETATION

Radio Science, Volume 18, Number 4, pages 557-565, July-August 1983

Scattering from randomly oriented circular discs with application to vegetation

M. A. Karam and A. K. Fung

Remote Sensing Laboratory, University of Kansas Center for Research, Inc.
Lawrence, Kansas 66045

(Received October 26, 1982; revised March 8, 1983; accepted March 8, 1983.)

A vegetation layer is modeled by a collection of randomly oriented circular discs over a half space. The backscattering coefficient from such a half space is computed using the radiative transfer theory. It is shown that significantly different results are obtained from this theory as compared with some earlier investigations using the same modeling approach but with restricted disc orientations. In particular, the backscattered cross-polarized returns cannot have a fast increasing angular trend which is inconsistent with measurements. By setting the appropriate angle of orientation to zero the theory reduces to previously published results. Comparisons are shown with measurements taken from milo, corn and wheat and good agreements are obtained for both polarized and cross-polarized returns.

1. INTRODUCTION

The problem of scattering from randomly oriented scatterers with application to vegetation has received much attention in recent years. The radiative transfer theory has been used to calculate the backscattering from a layer of randomly oriented ellipsoids with application to vegetation [Tsang et al., 1981]. Foldy's method and the distorted Born approximation have been used to calculate the backscattering cross section for randomly oriented circular discs in a half space [Lang, 1981]. The major advantage of this approach is that most of the model parameters are directly related to ground truth measurements.

In this study we use the scattering amplitude formula by Karam and Fung [1982a] for randomly oriented scatterers of arbitrary shape to derive the scattering amplitudes for randomly oriented circular discs. Then the phase matrix elements and the extinction coefficients are derived. These quantities are needed in the first-order radiative transfer theory for computing scattering from a half-space medium containing randomly oriented sparsely distributed lossy dielectric discs used to model a vegetated medium. In this model the effect of air-vegetation boundary is neglected due to the sparse distribution of the leaves. The decay of the incident wave in the vegetated volume is accounted for by the extinction coefficient which is related to the scattering amplitudes in the forward direction [Ishimaru and Cheung, 1980; Karam and Fung, 1982b].

The main difference between this study and those of Tsang et al. [1981] and Lang [1981] is that our formulation permits the circular discs to be oriented in any direction and accounts for changes in polarization of the scattered field due to changes in orientations of the circular discs. This difference is illustrated numerically in section 5 where comparisons with measured data on wheat, corn and milo [Dobson et al., 1977] are also shown.

Paper number 3S0419.
0048-6604/83 0708-0419$08.00

2. THE SCATTERING AMPLITUDE MATRIX AS A SPECIAL CASE OF THAT OF ELLIPSOIDS

Consider a randomly oriented ellipsoid with its semiaxes (a,b,c) aligned along the coordinates $(\hat{x}',\hat{y}',\hat{z}')$ of a local frame related to the principal frame $(\hat{x},\hat{y},\hat{z})$ through the angles of rotations (α,β,γ) with respect to the $\hat{z}'$, $\hat{y}'$ and $\hat{x}'$ axes, respectively (called the xyz convention by Goldstein [1981]) [Karam and Fung, 1982a]. Thus,

$$\hat{x}' = \cos\beta\cos\alpha\hat{x} + \cos\beta\sin\alpha\hat{y} - \sin\beta\hat{z} \quad (1)$$

$$\hat{y}' = (\cos\alpha\sin\beta\sin\gamma - \sin\alpha\cos\gamma)\hat{x} + (\cos\alpha\cos\gamma + \sin\alpha\sin\beta\sin\gamma)\hat{y} + \cos\beta\sin\gamma\hat{z} \quad (2)$$

$$\hat{z}' = (\sin\alpha\sin\gamma + \cos\alpha\sin\beta\cos\gamma)\hat{x} - (\cos\alpha\sin\gamma - \sin\alpha\sin\beta\cos\gamma)\hat{y} + \cos\beta\cos\gamma\hat{z} \quad (3)$$

For an incident plane wave in the $\hat{k}_i$ direction the polarization vectors ($\hat{v}_i$ and $\hat{h}_i$) in the principal frame, and the corresponding polarization vectors in the local frame ($\hat{v}_i'$ and $\hat{h}_i'$) can be expressed as

$$\hat{h}_i = \hat{z} \times \hat{k}_i / |\hat{z} \times \hat{k}_i| \qquad \hat{v}_i = \hat{h}_i \times \hat{k}_i \quad (4a)$$

$$\hat{h}_i' = \hat{z}' \times \hat{k}_i / |\hat{z}' \times \hat{k}_i| \qquad \hat{v}_i' = \hat{h}_i' \times \hat{k}_i \quad (4b)$$

where

$$\hat{k}_i = \sin\theta_i\cos\phi_i\hat{x} + \sin\theta_i\sin\phi_i\hat{y} + \cos\theta_i\hat{z} \quad (4c)$$

To relate $\hat{h}_i'$, $\hat{v}_i'$ to $\hat{h}_i$, $\hat{v}_i$ we express the principal frame in terms of $\hat{k}_i$, $\hat{v}_i$ and $\hat{h}_i$ as

$$\hat{x} = \sin\theta_i\cos\phi_i\hat{k}_i + \cos\theta_i\cos\phi_i\hat{v}_i - \sin\phi_i\hat{h}_i \quad (5a)$$

$$\hat{y} = \sin\theta_i\sin\phi_i\hat{k}_i + \cos\theta_i\sin\phi_i\hat{v}_i + \cos\phi_i\hat{h}_i \quad (5b)$$

$$\hat{z} = \cos\theta_i\hat{k}_i - \sin\theta_i\hat{v}_i \quad (5c)$$

Then substituting (5a)-(5c) into (3) we get

$$\hat{z}' = t_{ki}\hat{k}_i + t_{vi}\hat{v}_i + t_{hi}\hat{h}_i \quad (6)$$

where

$$t_{ki} = [\sin(\alpha-\phi_i)\sin\gamma + \cos(\alpha-\phi_i)\sin\beta\cos\gamma] \cdot \sin\theta_i + \cos\beta\cos\gamma\cos\theta_i \quad (7a)$$

$$t_{vi} = [\sin(\alpha-\phi_i)\sin\gamma + \cos(\alpha-\phi_i)\sin\beta\cos\gamma] \cdot \cos\theta_i - \cos\beta\cos\gamma\sin\theta_i \quad (7b)$$

$$t_{hi} = \sin(\alpha-\phi_i)\sin\beta\cos\gamma - \cos(\alpha-\phi_i)\sin\gamma \quad (7c)$$

Now substituting (6) into (4b) we get

$$\hat{v}_i' = \frac{1}{\sqrt{t_{vi}^2 + t_{hi}^2}} [-t_{vi}\hat{v}_i - t_{hi}\hat{h}_i] \quad (8a)$$

$$\hat{h}_i' = \frac{1}{\sqrt{t_{vi}^2 + t_{hi}^2}} [t_{hi}\hat{v}_i - t_{vi}\hat{h}_i] \quad (8b)$$

Relations similar to (4)-(8) can be written for the scattered wave by replacing the subscript i with s. (Note that the orientation of the scatterer and its effect on the polarization of the scattered field are not represented in the most general form when the local frame is described by the Eulerian angles of rotation (appendix).)

Under the low frequency approximation [Stratton, 1941; Stevenson, 1953; Ruck et al., 1970; Ishimaru, 1978; Tsang et al., 1981] the scattering amplitudes for the ellipsoid in the local frame can be written as

$$f_{vv}'(\hat{s},\hat{i}) = \frac{\omega^2\mu}{4\pi} V_0(\epsilon_s-\epsilon)\left[\frac{(\hat{v}_s'\cdot\hat{x}')(\hat{v}_i'\cdot\hat{x}')}{\nu A_a + 1} + \frac{(\hat{v}_s'\cdot\hat{y}')(\hat{v}_i'\cdot\hat{y}')}{1} + \frac{(\hat{v}_s'\cdot\hat{z}')(\hat{v}_i'\cdot\hat{z}')}{\nu A_c + 1}\right] \quad (9)$$

$$f'_{vh}(\hat{s},\hat{i}) = \frac{\omega^2\mu}{4\pi}V_0(\varepsilon_s-\varepsilon)\left[\frac{(\hat{v}_s'\cdot\hat{x}')(\hat{h}_i'\cdot\hat{x}')}{\nu A_a+1} + \frac{(\hat{v}_s'\cdot\hat{y}')(\hat{h}_i'\cdot\hat{y}')}{\nu A_b+1} + \frac{(\hat{v}_s'\cdot\hat{z}')(\hat{h}_i'\cdot\hat{z}')}{\nu A_c+1}\right] \quad (10)$$

$$f'_{hv}(\hat{s},\hat{i}) = \frac{\omega^2\mu}{4\pi}V_0(\varepsilon_s-\varepsilon)\left[\frac{(\hat{h}_s'\cdot\hat{x}')(\hat{v}_i'\cdot\hat{x}')}{\nu A_a+1} + \frac{(\hat{h}_s'\cdot\hat{y}')(\hat{v}_i'\cdot\hat{y}')}{\nu A_b+1} + \frac{(\hat{h}_s'\cdot\hat{z}')(\hat{v}_i'\cdot\hat{z}')}{\nu A_c+1}\right] \quad (11)$$

$$f'_{hh}(\hat{s},\hat{i}) = \frac{\omega^2\mu}{4\pi}V_0(\varepsilon_s-\varepsilon)\left[\frac{(\hat{h}_s'\cdot\hat{x}')(\hat{h}_i'\cdot\hat{x}')}{\nu A_a+1} + \frac{(\hat{h}_s'\cdot\hat{y}')(\hat{h}_i'\cdot\hat{y}')}{\nu A_b+1} + \frac{(\hat{h}_s'\cdot\hat{z}')(\hat{h}_i'\cdot\hat{z}')}{\nu A_c+1}\right] \quad (12)$$

where the third term in (10)-(12) is zero since $(\hat{h}_i'\cdot\hat{z}')=(\hat{h}_s'\cdot\hat{z}')=0$; ω is the angular frequency of the incident wave; ε_s is the permittivity of the scatterer; ε is the permittivity of the surrounding medium; and $V_0=(4\pi abc/3)$ is the volume of the scatterer. In (9)-(12) we also have

$$\nu = \frac{abc}{2}\left(\frac{\varepsilon_s}{\varepsilon}-1\right)$$

$$R(u) = \left[(u+a^2)(u+b^2)(u+c^2)\right]^{\frac{1}{2}}$$

$$A_a = \int_0^\infty \frac{du}{(a^2+u)R(u)}$$

$$A_b = \int_0^\infty \frac{du}{(b^2+u)R(u)}$$

$$A_c = \int_0^\infty \frac{du}{(c^2+u)R(u)}$$

When a=b and c<<a the ellipsoid can be approximated as a circular disc with radius a and thickness 2c. In this limit [Tsang et al., 1981] we have

$$A_a = A_b = \frac{\pi}{2a^3} \qquad A_c = \frac{2}{a^2c}$$

Hence,

$$\nu A_a = \nu A_b = \left(\frac{\varepsilon_s}{\varepsilon}-1\right)\frac{\pi c}{4a} \qquad \nu A_c = \left(\frac{\varepsilon_s}{\varepsilon}-1\right)$$

Let us define

$$a_T = \frac{(\varepsilon_s/\varepsilon-1)}{\nu A_a+1} \qquad a_N = \frac{(\varepsilon_s/\varepsilon-1)}{\nu A_c+1} \qquad C_0 = \frac{\omega^2\mu\varepsilon}{4\pi}V_0$$

We can now write the element of the scattering amplitude matrix for a circular disc in the local frame as a special case of (9)-(12).

$$f'_{vv}(\hat{s},\hat{i}) = C_0[(\hat{v}_s'\cdot\hat{v}_i')a_T + (\hat{v}_s'\cdot\hat{z}')(\hat{v}_i'\cdot\hat{z}')(a_N-a_T)] \quad (13)$$

$$f'_{vh}(\hat{s},\hat{i}) = C_0[(\hat{v}_s'\cdot\hat{h}_i')a_T + (\hat{v}_s'\cdot\hat{z}')(\hat{h}_i'\cdot\hat{z}')(a_N-a_T)] \quad (14)$$

$$f'_{hv}(\hat{s},\hat{i}) = C_0[(\hat{h}_s'\cdot\hat{v}_i')a_T + (\hat{h}_s'\cdot\hat{z}')(\hat{v}_i'\cdot\hat{z}')(a_N-a_T)] \quad (15)$$

$$f'_{hh}(\hat{s},\hat{i}) = C_0[(\hat{h}_s'\cdot\hat{h}_i')a_T + (\hat{h}_s'\cdot\hat{z}')(\hat{h}_i'\cdot\hat{z}')(a_N-a_T)] \quad (16)$$

In view of (8) an incident field amplitude in the principal frame can be expressed in the local frame where scattering takes place in accordance with (13)-(16). Then a similar relation to (8) may be applied to convert the scattering field back to the principal frame [Karam and Fung, 1982a]. Thus,

$$f_{vv}(\hat{s},\hat{i}) = [t_{vs}f'_{vv}(\hat{s},\hat{i})t_{vi} - t_{vs}f'_{vh}(\hat{s},\hat{i})t_{hi} - t_{hs}f'_{hv}(\hat{s},\hat{i})t_{vi} + t_{vs}f'_{hh}(\hat{s},\hat{i})t_{hi}]/D(\hat{s},\hat{i}) \quad (17)$$

$$f_{vh}(\hat{s},\hat{i}) = [t_{vs}f'_{vv}(\hat{s},\hat{i})t_{hi}+t_{vs}f'_{vh}(\hat{s},\hat{i})t_{vi} -t_{hs}f'_{hv}(\hat{s},\hat{i})t_{hi}-t_{hs}f'_{hh}(\hat{s},\hat{i})t_{vi}]/D(\hat{s},\hat{i}) \quad (18)$$

$$f_{hv}(\hat{s},\hat{i}) = [t_{hs}f'_{vv}(\hat{s},\hat{i})t_{vi}+t_{vs}f'_{hv}(\hat{s},\hat{i})t_{vi} -t_{hs}f'_{vh}(\hat{s},\hat{i})t_{hi}-t_{vs}f'_{hh}(\hat{s},\hat{i})t_{hi}]/D(\hat{s},\hat{i}) \quad (19)$$

$$f_{hh}(\hat{s},\hat{i}) = [t_{hs}f'_{vv}(\hat{s},\hat{i})t_{hi}+t_{vs}f'_{hv}(\hat{s},\hat{i})t_{hi} +t_{hs}f'_{vh}(\hat{s},\hat{i})t_{vi}+t_{vs}f'_{hh}(\hat{s},\hat{i})t_{vi}]/D(\hat{s},\hat{i}) \quad (20)$$

where

$$D(\hat{s},\hat{i}) = \left[\left(t_{vi}^2+t_{hi}^2\right)\left(t_{hs}^2+t_{vs}^2\right)\right]^{1/2} \quad (21)$$

Equations (17)-(21) will be used in the following sections to calculate the first-order scattering cross section for a half space of randomly oriented circular discs.

3. FIRST-ORDER SCATTERING CROSS SECTION FOR A HALF SPACE OF RANDOMLY ORIENTED CIRCULAR DISCS

For a collection of identical randomly oriented lossy dielectric circular discs embedded in the lower half space, the backscattering cross section [Tsang and Kong, 1978; Tsang et al., 1981] based on the first-order solution of the radiative transfer equation [Karam and Fung, 1982c] can be written as

$$\sigma_{vv}(-\hat{i},\hat{i}) = \frac{2\pi}{\lambda}\frac{\cos\theta_i}{\mathrm{Im}\langle f_{vv}(\hat{i},\hat{i})\rangle+\mathrm{Im}\langle f_{vv}(-\hat{i},-\hat{i})\rangle} \cdot \langle|f_{vv}(-\hat{i},\hat{i})|^2\rangle \quad (22)$$

$$\sigma_{vh}(-\hat{i},\hat{i}) = \frac{2\pi}{\lambda}\frac{\cos\theta_i}{\mathrm{Im}\langle f_{vv}(\hat{i},\hat{i})\rangle+\mathrm{Im}\langle f_{hh}(-\hat{i},-\hat{i})\rangle} \cdot \langle|f_{vh}(-\hat{i},\hat{i})|^2\rangle \quad (23)$$

$$\sigma_{hh}(-\hat{i},\hat{i}) = \frac{2\pi}{\lambda}\frac{\cos\theta_i}{\mathrm{Im}\langle f_{hh}(\hat{i},\hat{i})\rangle+\mathrm{Im}\langle f_{hh}(-\hat{i},-\hat{i})\rangle} \cdot \langle|f_{hh}(-\hat{i},\hat{i})|^2\rangle \quad (24)$$

where λ is the wavelength of the incident wave, Im( ) is the imaginary part operator and the angle brackets are the ensemble average symbol over the orientation and distribution of the scatterer.

4. THE ENSEMBLE AVERAGE OVER THE ANGLES OF ORIENTATION FOR FORWARD AND BACKSCATTERING

In the forward direction, $\hat{k}_s=\hat{k}_i$; hence, $\hat{h}_s=\hat{h}_i$, $\hat{v}_s=\hat{v}_i$, $\hat{v}_s'=\hat{v}_i'$ and $\hat{h}_s'=\hat{h}_i'$. Similar statements can be made about t_{vi}, t_{hi} and t_{vs}, t_{hs}.

In the backscattering direction similar results are obtained as in the forward direction except that $\hat{h}_s'$ and t_{hs} will differ in sign from those in the forward direction.

From the above discussion the forward and backscattering scattering amplitudes in the local frame (13)-(16) reduce to

$$f'_{vv}(\pm\hat{i},\hat{i}) = C_0\left[a_T+(\hat{v}_i'\cdot\hat{z}')^2(a_N-a_T)\right] \quad (25)$$

$$f'_{vh}(\pm\hat{i},\hat{i}) = f'_{hv}(\pm\hat{i},\hat{i}) = 0 \quad (26)$$

$$f'_{hh}(\pm\hat{i},\hat{i}) = \pm C_0\left[a_T+(\hat{h}_i'\cdot\hat{z}')^2(a_N-a_T)\right] \quad (27)$$

Also, the scattering amplitudes in the principal frame described by (17)-(21) reduce to

$$f_{vv}(\pm\hat{i},\hat{i}) = C_0\left[a_T+t_{vi}^2(a_N-a_T)\right] \quad (28)$$

$$f_{vh}(\pm\hat{i},\hat{i}) = C_0\left[t_{hi}t_{vi}(a_N-a_T)\right] \quad (29)$$

$$f_{hv}(\pm\hat{i},\hat{i}) = \pm C_0\left[t_{hi}t_{vi}(a_N-a_T)\right] \quad (30)$$

$$f_{hh}(\pm\hat{i},\hat{i}) = C_0\left[a_T+t_{hi}^2(a_N-a_T)\right] \quad (31)$$

To calculate the backscattering cross section in (22)-(24) we first substitute (7) in (28)-(31) and then we calculate

the ensemble average of the quantities $\langle f_{vv}(\hat{i},\hat{i})\rangle$, $\langle f_{hh}(\hat{i},\hat{i})\rangle$, $\langle|f_{vv}(-\hat{i},\hat{i})|^2\rangle$, $\langle|f_{hh}(-\hat{i},\hat{i})|^2\rangle$, and $\langle|f_{vh}(-\hat{i},\hat{i})|^2\rangle$.

Due to the symmetry of the disc we will assume an equally likely distribution function with respect to α. The ensemble average over α will remove the ϕ_i dependence, yielding

$$\langle f_{vv}(\pm\hat{i},\pm\hat{i})\rangle = C_0 n_0\left[a_T + \int_0^{\pi/2} p(\beta)\, d\beta \cdot \int_0^{\pi/2} p(\gamma)\, d\gamma \left\{\left(\tfrac{1}{2}\sin^2\beta\cos^2\theta_i + \cos^2\beta\sin^2\theta_i\right)\cdot \cos^2\gamma + \tfrac{1}{2}\cos^2\theta_i\sin^2\gamma\right\}(a_N - a_T)\right] \tag{32}$$

$$\langle f_{hh}(\pm\hat{i},\pm\hat{i})\rangle = C_0 n_0\left[a_T + \int_0^{\pi/2} p(\beta)\, d\beta \cdot \int_0^{\pi/2} p(\gamma)\, d\gamma \left\{\tfrac{1}{2}\left(\sin^2\beta\cos^2\gamma + \sin^2\gamma\right)\right\}\cdot (a_N - a_T)\right] \tag{33}$$

$$\langle|f_{vv}(-\hat{i},\hat{i})|^2\rangle = C_0^2 n_0\left[|a_T|^2 + \int_0^{\pi/2} p(\beta)\, d\beta \cdot \int_0^{\pi/2} p(\gamma)\, d\gamma \left\{2\left(\left(\tfrac{1}{2}\sin^2\beta\cos^2\theta_i + \cos^2\beta\sin^2\theta_i\right)\cos^2\gamma + \tfrac{1}{2}\cos^2\theta_i\sin^2\gamma\right)\mathrm{Re}\left(a_T^*(a_N - a_T)\right) + \left(\tfrac{3}{8}\cos^4\theta_i\sin^4\gamma + \left(\sin^4\theta_i\cos^4\beta + \tfrac{3}{8}\cos^4\theta_i\sin^4\beta + \tfrac{3}{16}\sin^2 2\theta_i\sin^2 2\beta\right)\cos^4\gamma + \tfrac{3}{16}\left(\cos^4\theta_i\sin^2\beta + \sin^2 2\theta_i\cos^2\beta\right)\sin^2 2\gamma\right)\cdot |a_N - a_T|^2\right\}\right] \tag{34}$$

$$\langle|f_{hh}(-\hat{i},\hat{i})|^2\rangle = C_0^2 n_0\left[|a_T|^2 + \int_0^{\pi/2} p(\beta)\, d\beta \cdot \int_0^{\pi/2} p(\gamma)\, d\gamma \left\{\left(\sin^2\beta\cos^2\gamma + \sin^2\gamma\right)\mathrm{Re}\left(a_T^*(a_N - a_T)\right) + \tfrac{3}{8}\left(\sin^4\beta\cos^4\gamma + \tfrac{1}{2}\sin^2\beta\sin^2 2\gamma + \sin^4\gamma\right)|a_N - a_T|^2\right\}\right] \tag{35}$$

$$\langle|f_{vh}(-\hat{i},\hat{i})|^2\rangle = \frac{C_0^2 n_0}{8}\left[\int_0^{\pi/2} p(\beta)\, d\beta \cdot \int_0^{\pi/2} p(\gamma)\, d\gamma \left\{\left(\cos^2\theta_i\sin^4\beta + \sin^2 2\beta\sin^2\theta_i\right)\cdot \cos^4\gamma + \cos^2\theta_i\sin^4\gamma + \left(\tfrac{1}{2}\sin^2\beta\cos^2\theta_i + \cos^2\beta\sin^2\theta_i\right)\sin^2 2\gamma\right\}|a_N - a_T|^2\right] \tag{36}$$

where n_0 is the number of the scatterers per unit volume; $p(\beta)$ and $p(\gamma)$ are the orientation probabilities with respect to β and γ, respectively: Re( ) is the real part operator and the asterisk is the complex conjugate symbol. The integration with respect to β and γ is taken over $\pi/2$ due to the symmetry of the disc. From (32)-(36) we note that n_0 appears in both the numerator and denominator of (22)-(24) so it will be canceled out.

5. NUMERICAL RESULTS AND DISCUSSION

To compare our formulation with that in the literature [Lang, 1981; Tsang et al., 1981] and to show the agreement between this theory and some measured data [Dobson et al., 1977] we will assume an orientation distribution function with respect to β and γ as

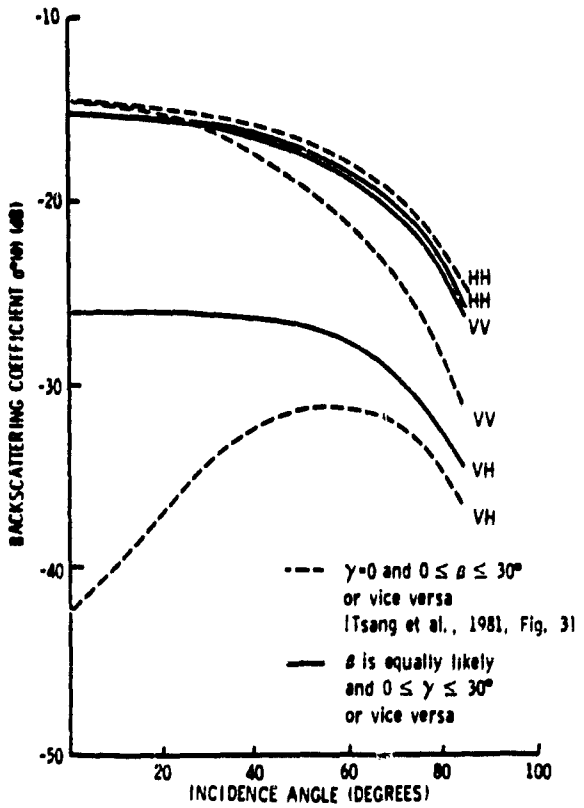

Fig. 1. A comparison with Tsang et al. [1981] (f=1.1 GHz; a=10 mm; c=0.375 mm; ϵ_r=30.8+j1.8).

$$p(\Omega) = \begin{cases} \dfrac{1}{\Omega_2-\Omega_1} & \Omega_1<\Omega<\Omega_2 \\ 0 & \text{otherwise} \end{cases} \qquad (37)$$

with $\Omega=\beta$ and γ. Also, we assume that the discs have a dielectric constant based on the formula given by Fung and Ulaby [1978].

In our formulation we have the freedom to select different distribution functions with respect to β and γ and we note the following:

1. When we set γ equal to zero our formulation reduces to those derived by Tsang et al. [1981] and Lang [1981]. In Figure 1 a case shown in the work by Tsang et al. [1981] is reproduced. It is seen that when γ is not restricted to zero, substantially different σ^o_{VV} and σ^o_{HV} are obtained. Since naturally occurring leaves are, in general, not restricted in their orientation, we believe that both γ and β should be permitted to vary. In Figure 2 another case is illustrated which shows that the relative levels of σ^o_{VV} and σ^o_{HH} are interchanged and σ^o_{VH} has a higher level and a different angular behavior as compared to those reported by Lang [1981], when both γ and β are assumed equally likely distributed.

2. The roles of γ and β may be interchanged without affecting the σ^o computation, if they are assumed to have the same distribution (see Figures 1-5). This is expected since β measures tilting in the x' direction, while γ measures tilting in the y' direction, respectively.

3. When the discs are oriented more

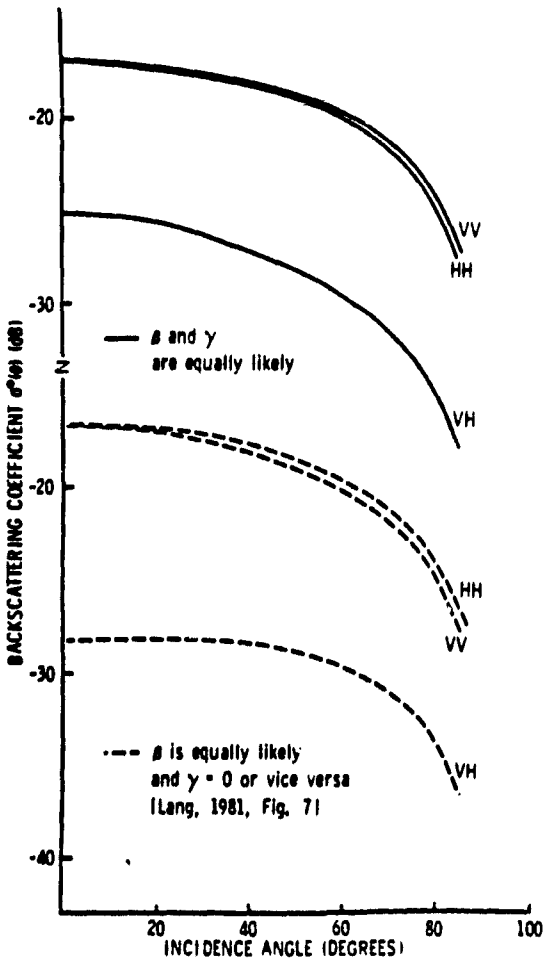

Fig. 2. A comparison with Lang [1981] (f=1.1 GHz; a=10 mm; c=0.25 mm; ϵ_r=31+j1.8).

nearly horizontal, we get $\sigma^o_{HH} > \sigma^o_{VV}$ (Figure 1). When the discs are oriented more nearly vertical, $\sigma^o_{VV} > \sigma^o_{HH}$ (Figures 3-5).

In Figures 3-5, comparisons with measurements at large angles of incidence are shown (30°-80°). This angular range is selected to avoid the ground effect in backscattering. In the case of corn and milo, it is known that these crops have large leaves which do bend and twist in their natural state. As a result, one leaf may have several scattering centers and, hence, is modeled by several discs. The leaf thickness, however, should correspond to disc thickness in modeling. Of course, the dielectric property of the leaf must be directly applicable in modeling also. Figures 3-5 show that the leaves of these crops are more nearly vertical than horizontal and that among the crops considered, the leaf volume is the largest for corn and the smallest for wheat. Reasonable level and trend agreements are obtained in Figures 3-5 in both like and cross polarizations.

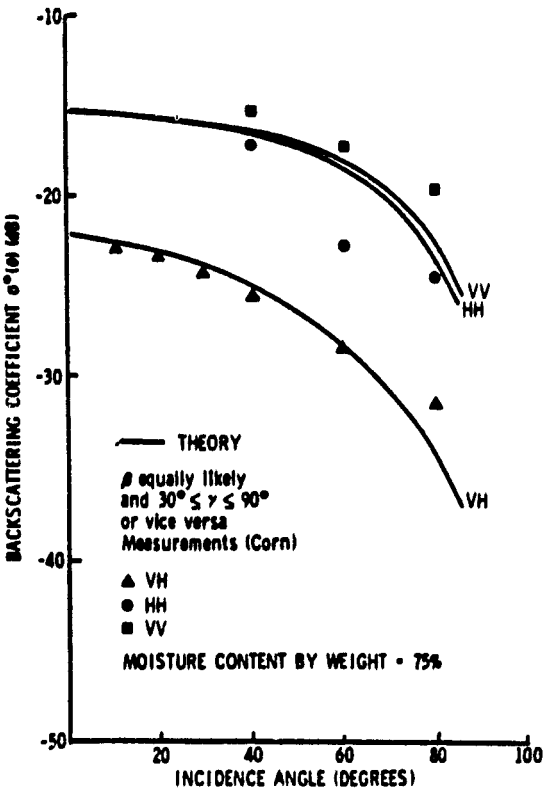

Fig. 3. Comparison with measurements of corn (f=1.1 GHz; a=15 mm; c=0.167 mm; ε_r=30.8+j1.8).

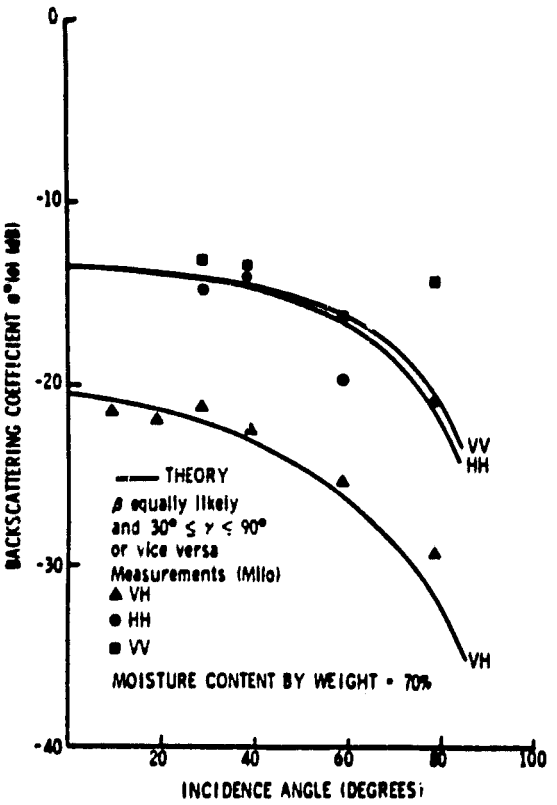

Fig. 4. Comparison with measurements of milo (f=1.5 GHz; a=12.3 mm; c=0.2 mm; ε_r=28.52+j2.13).

6. CONCLUSIONS

By permitting arbitrary orientation in modeling, reasonable agreements are obtained between theory and low frequency data (1.1-1.5 GHz) collected from corn, milo and wheat. It is shown that when the orientation of the leaves is restricted [Lang, 1981; Tsang et al., 1981], the levels of σ^o_{VV} and σ^o_{HH} are interchanged and, hence, cannot produce agreement with these crop data.

APPENDIX: THE EULERIAN ANGLES OF ROTATION AS A LOCAL FRAME

The coordinates described by the Eulerian angles of rotation are obtained by three

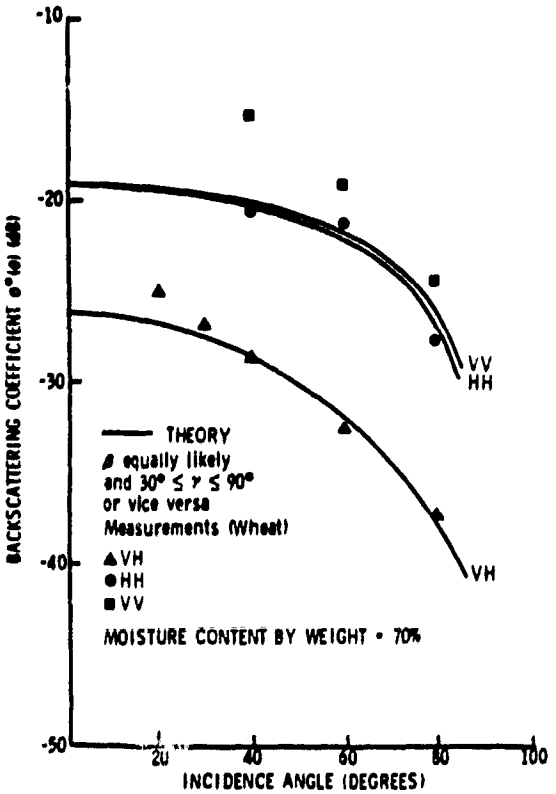

Fig. 5. Comparison with measurements of wheat (f=1.5 GHz; a=10 mm; c=0.087 mm; ϵ_r=28.52+j2.13).

successive rotations around the $\hat{z}$ axis, the y axis and then the $\hat{z}$ axis again with angles α, β, and γ, respectively (called the y convention by Goldstein [1981]). The resulting coordinates can be written as [Arfken, 1970]

$$\hat{x}' = (\cos\gamma\cos\beta\cos\alpha - \sin\gamma\sin\alpha)\hat{x} + (\cos\gamma\cos\beta\sin\alpha + \sin\gamma\cos\alpha)\hat{y} - \cos\gamma\sin\beta\hat{z} \quad (A1)$$

$$\hat{y}' = -(\sin\gamma\cos\beta\cos\alpha + \cos\gamma\sin\alpha)\hat{x} + (-\sin\gamma\cos\beta\sin\alpha + \cos\gamma\cos\alpha)\hat{y} + \sin\gamma\sin\beta\hat{z} \quad (A2)$$

$$\hat{z}' = \sin\beta\cos\alpha\hat{x} + \sin\beta\sin\alpha\hat{y} + \cos\beta\hat{z} \quad (A3)$$

If we use the coordinates described by (A1), (A2) and (A3) as a local frame to describe the orientation of the scatterers, we can substitute (5) into (A3). This gives an expression similar to (6), i.e.,

$$\hat{z}' = t_{ki}\hat{k}_i + t_{vi}\hat{v}_i + t_{hi}\hat{h}_i \quad (A4)$$

where

$$t_{ki} = \sin\beta\sin\theta_i\cos(\alpha-\phi_i) + \cos\beta\cos\theta_i \quad (A5)$$

$$t_{vi} = \sin\beta\cos\theta_i\cos(\alpha-\phi_i) - \cos\beta\sin\theta_i \quad (A6)$$

$$t_{hi} = \sin\beta\sin(\alpha-\phi_i) \quad (A7)$$

We see from (A6) and (A7) that they are independent of angle γ. Hence, when we use (8) to represent the polarization vectors in the local frame in terms of the polarization vectors in the principal frame, the system depends only on α and β. In fact (A6) and (A7) are a special case of (7b) and (7c) when γ=0 and only two of the three angles α, β, and γ are independent in the Eulerian description. Using the spherical coordinates to describe the local frame of the scatterer [Lang, 1981, Figure 3] will lead to the same result as the Eulerian angles of rotation with $\hat{r}$, ϕ, and θ corresponding to $\hat{z}'$, α, and β, respectively.

Another simple way to see the difference between the xyz and y conventions is to consider the special case β=0. Then the xyz convention in (1)-(3) gives

$$\hat{x}' = \cos\alpha\hat{x} + \sin\alpha\hat{y} \quad (A8)$$

$$\hat{y}' = -\sin\alpha\cos\gamma\hat{x} + \cos\alpha\cos\gamma\hat{y} + \sin\gamma\hat{z} \quad (A9)$$

$$\hat{z}' = \sin\alpha\sin\gamma\hat{x} - \cos\alpha\sin\gamma\hat{y} + \cos\gamma\hat{z} \quad (A10)$$

and the y convention in (A1)-(A3) gives

$$\hat{x}' = \cos(\alpha+\gamma)\hat{x} + \sin(\alpha+\gamma)\hat{y} \quad (A11)$$

$$\hat{y}' = -\sin(\alpha+\gamma)\hat{x} + \cos(\alpha+\gamma)\hat{y} \quad (A12)$$

$$\hat{z}' = \hat{z} \quad (A13)$$

Thus the y convention depends only on one angle, $\alpha+\gamma$, while the xyz convention still depends on two angles α and γ.

Acknowledgments. This work was supported in part by the U.S. Army Research Office under grant DAAG29-80-K-0018 and in part by NASA Goddard Space Flight Center under grant NAG5-268.

REFERENCES

Arfken, G., Mathematical Methods for Physicists, pp. 178-180, Academic, New York, 1970.

Dobson, C., H. Stiles, D. Brunfeldt, T. Metzler, and S. McMeckin, Data documentation: 1976 MAS 1-8 and MAS 8-18 vegetation experiments, Tech. Rep. RSL TR 264-15, Remote Sens. Lab., Univ. of Kans., Center for Res., Inc., Lawrence, Kans., 1977.

Fung, A. K., and F. T. Ulaby, A scatter model for leafy vegetation, IEEE Trans. Geosci. Electron., 16, 281-286, 1978.

Goldstein, H., Classical Mechanics, pp. 143-148, 606-610, Addison-Wesley, Reading, Mass., 1981.

Ishimaru, A., Wave Propagation and Scattering in Random Media, vol. 1, pp. 20-22, Academic, New York, 1978.

Ishimaru, A., and R. Cheung, Multiple scattering effects on wave propagation due to rain, Ann. Telecommun., 35, 11-12, 1980.

Karam, M. A., and A. K. Fung, The scattering matrix for an arbitrarily oriented scatterer of arbitrary shape, Tech. Rep. RSL TR 435-5, Remote Sens. Lab., Univ. of Kans., Center for Res., Inc., Lawrence, Kans, 1982a.

Karam, M. A., and A. K. Fung, Vector forward scattering theorem, Radio Sci., 17, 752-756, 1982b.

Karam, M. A., and A. K. Fung, Propagation and scattering in multi-layered random media with rough interfaces, J. Electromagn., 2, 239-256, 1982c.

Lang, L. H., Electromagnetic backscattering from a sparse distribution of lossy dielectric scatterers, Radio Sci., 16, 15-30, 1981.

Ruck, G. T., D. E. Barrick, W. D. Stuart, and C. K. Krichbaum, Radar Cross-Section Handbook, vol. 1, pp. 297-299, McGraw-Hill, New York, 1970.

Stevenson, A. F., Electromagnetic scattering by an ellipsoid in the third approximation, J. Appl. Phys., 24, 1143-1151, 1953.

Stratton, J. A., Electromagnetic Theory, pp. 207-213, McGraw-Hill, New York, 1941.

Tsang, L., and J. A. Kong, Radiative transfer theory for active remote sensing of half-space random media, Radio Sci., 13, 763-773, 1978.

Tsang, L., M. C. Kubasci, and J. A. Kong, Radiative transfer theory for active remote sensing of a layer of small ellipsoidal scatterers, Radio Sci., 16(3), 321-329, 1981.

APPENDIX E

A COMPARISON BETWEEN ACTIVE AND PASSIVE SENSING OF SOIL MOISTURE FROM VEGETATED TERRAINS

A COMPARISON BETWEEN ACTIVE AND PASSIVE SENSING OF SOIL MOISTURE FROM VEGETATED TERRAINS

A. K. Fung and H. J. Eom
Remote Sensing Laboratory
University of Kansas
Lawrence, Kansas, USA 66045

ABSTRACT

A comparison between active and passive sensing of soil moisture over vegetated areas is studied via scattering models. In active sensing three contributing terms to radar backscattering can be identified: (1) the ground surface scatter term; (2) the volume scatter term representing scattering from the vegetation layer; and (3) the surface-volume scatter term accounting for scattering from both surface and volume. In emission three sources of contribution can also be identified: (1) surface emission, (2) upward volume emission from the vegetation layer, and (3) downward volume emission scattered upward by the ground surface. As ground moisture increases, terms (1) and (3) increase due to increase in permittivity in the active case. However, in passive sensing, term (1) decreases but term (3) increases for the same reason. This self-compensating effect produces a loss in sensitivity to change in ground moisture. Furthermore, emission from vegetation may be larger than that from the ground. Hence, the presence of vegetation layer causes a much greater loss of sensitivity to passive than active sensing of soil moisture.

1.0 INTRODUCTION

Theories on intensity scattering [1,2] and emission [3,4] have been developed for an inhomogeneous layer with irregular boundaries. To model a leafy vegetation layer above an irregular ground surface the phase function for a dielectric disk is needed (Appendix A) and the top layer boundary may be removed [5]. Such a model is expected to be valid for vegetated medium where scattering is dominated by leaves. Note that a real leaf is, in general, not a flat disk but is curved and may twist, especially if it is long. Hence, a dielectric disk will model a scattering center on a leaf and a long leaf may have several scattering centers.

For soil moisture sensing only polarized scattering has been used in practice [6]. It is also known from experimental studies that the albedo of a vegetated medium is usually around 0.3 or less [7,8]. This means that a first-order solution of the radiative transfer equation obtained by assuming a weak scattering medium can provide useful estimates. The computational procedure to obtain the first-order solutions for both the active and passive problems are outlined in the next two sections. The relevant characteristics of the scattering model is given in Section 4 and those of the emission model in Section 5. Comparisons with measurments are shown in Section 6.

2.0 THE FIRST-ORDER SOLUTION FOR THE ACTIVE PROBLEM

Let us assume that the radiative transfer equations for the upward and downward intensities, $\bar{I}^+$ and $\bar{I}^-$, are applicable within the vegetation layer (Fig. 1)

$$\mu_s \frac{d\bar{I}^+}{dz} = -\bar{K}_e \bar{I}^+ + \frac{\bar{K}_s}{4\pi} \int_0^{2\pi} \int_0^1 \bar{P}(\mu_s, \mu, \phi_s - \phi)\, \bar{I}^+ \, d\mu \, d\phi$$

$$+ \frac{\bar{K}_s}{4\pi} \int_0^{2\pi} \int_0^1 \bar{P}(\mu_s, -\mu, \phi_s - \phi)\, \bar{I}^- \, d\mu \, d\phi \,, \qquad (1)$$

$$-\mu_s \frac{d\bar{I}^-}{dz} = -\bar{K}_e \bar{I}^- + \frac{\bar{K}_s}{4\pi} \int_0^{2\pi} \int_0^1 \bar{P}(-\mu_s, \mu, \phi_s - \phi)\, \bar{I}^+ \, d\mu \, d\phi$$

$$+ \frac{\bar{K}_s}{4\pi} \int_0^{2\pi} \int_0^1 \bar{P}(-\mu_s, -\mu, \phi_s - \phi)\, \bar{I}^- \, d\mu \, d\phi \,, \qquad (2)$$

where $\bar{K}_s$, $\bar{K}_e$ are the volume scattering and extinction coefficient matrices, respectively,; $\mu_s = \cos\theta_s$, $\mu = \cos\theta$; and $\bar{P}(\ )$ is the phase matrix. We assume that the layer has no upper boundary and the boundary condition at the lower boundary is

$$\bar{I}^+(-d, \mu_s, \phi_s) = \frac{1}{4\pi} \int_0^{2\pi} \int_0^1 \bar{G}(\mu_s, \mu, \phi_s - \phi)\, \bar{I}^- \, d\mu \, d\phi \,, \qquad (3)$$

where $\bar{G}$ is the surface scattering phase matrix given in [2]. To account for polarization effects the intensity column matrices contain the four Stokes parameters as their elements [9]. Once the total scattered intensity for an α polarized component I_α^s of the intensity matrix at z=0 is found, the scattering coefficient for this component is defined relative to the incident

intensity I_β^i of polarization β as

$$\sigma^o_{\alpha\beta} = 4\pi \cos\theta_s \, I_\alpha^s / I_\beta^i \, . \tag{4}$$

The procedure to determine up to the first-order solution of (1) and (2) subject to (3) is as follows:

(a) Expand $\bar{P}$, $\bar{I}$ into Fourier series with respect to the azimuthal angle and consider one Fourier component at a time.

(b) Convert a Fourier component representation of (1) and (2) into integral equations.

(c) Use an N-point quadrature integration to rewrite the integrals with respect to μ in (1), (2), and (3) as a matrix product.

(d) Solve the resulting integral equations iteratively by assuming that $\bar{K}_s$ is small.

The m^{th} Fourier component of the scattering intensity including only the zeroth-order and the significant terms in the first-order is

$$\bar{I}^m = [\bar{f}_1 + \bar{N}^+ + (\bar{f}_1 \bar{N}^- + \bar{M} \bar{f}_1)] \, \bar{I}^{im} \, , \tag{5}$$

where $\bar{I}^{im}$ is the m^{th} Fourier coefficient of the incident intensity. In (5), $\bar{f}_1$ represents surface scattering attenuated by the layer,

$$\bar{f}_1 = e^{-\bar{K}_{epi} d} \, f_m \, \bar{G}^m \, e^{-\bar{K}_{epj} d} \, , \tag{6}$$

where $f_m = 1/2$, $m=0$, and $f_m = 1/4$, $m>0$, and $e^{-\bar{K}_{epi} d}$ is the diagonal matrix defined as

$$e^{-\bar{K}_{epi}d} = \text{Diag}\left[e^{-K_{e1}d/\cos\theta_1},\ldots, e^{-K_{e1}d/\cos\theta_N}, e^{-K_{e2}d/\cos\theta_1},\ldots,\right.$$

$$e^{-K_{e2}d/\cos\theta_N}, e^{-K_{e3}d/\cos\theta_1},\ldots, e^{-K_{e3}d/\cos\theta_N},$$

$$\left. e^{-K_{e4}d/\cos\theta_1},\ldots, e^{-K_{e4}d/\cos\theta_N}\right] \quad ,$$

$K_{e1} = K_{ev}$, extinction coefficient for vertical polarization,

$K_{e2} = K_{eh}$, extinction coefficient for horizontal polarization,

$K_{e3} = K_{e4} = (K_{e1} + K_{e2})/2$,

and p, i are the indices for the Stokes parameters and the quadrature points, respectively, and $\bar{G}^m$ is the m^{th} Fourier component of the surface scattering phase matrix [2]. $\bar{N}^+$ in (5) represents the volume scattering operator which scatters a downward propagating intensity upward. Its elements are defined in terms of the elements of the phase matrix for the pq polarization component as

$$(n^+_{pq})_{ij} = K_{spi}\, f_m\, p^m_{pq}(\mu_i,-\mu_j)\left[1 - e^{-(K_{epi}+K_{eqj})d}\right]$$

$$(K_{epi}+K_{eqj})^{-1} \quad , \qquad (7)$$

where $K_{spi} = K_{sp}/\mu_i$, K_{sp} is the volume scattering coefficient for p polarization, and $\mu_j = \cos\theta_j$. The index j is also for denoting quadrature points similar to i except it is used for the incoming polar angle direction. The last term in (5), $(\bar{\bar{M}}\bar{f}_1+\bar{f}_1\bar{N}^-)$, represents combined surface-volume scattering. The matrix elements of $\bar{M}$ for the pq polarization element is

$$(m_{pq})_{ij} = K_{spi}\, f_m\, p^m_{pq}(\mu_i,\mu_j)\left[1 - e^{-(K_{epi}-K_{eqj})d}\right] \qquad (8a)$$

$$(K_{epi}-K_{eqj})^{-1} \quad .$$

$\bar{M}$ may be interpreted as the volume scattering operator which scatters an upward propagating intensity upward. Similarly, $\bar{N}^-$ is the volume scattering operator which scatters a downward propagating intensity downward. Its elements are

$$(n^-_{pq})_{ij} = K_{spi}\, f_m\, p^m_{pq}(-\mu_i,-\mu_j)\left[e^{(K_{epi}-K_{eqj})d} - 1\right] \qquad (8b)$$

$$(K_{epi}-K_{eqj})^{-1} \quad .$$

Since we assume a weak scattering medium, the dominant term in (5) is (6), especially at small angles of incidence. On the other hand, the surface scattering matrix in (6) can be a fast decreasing function of the incidence angle θ. If observations were made at $\theta > 25°$ it is possible for the other terms in (5) to dominate. For soil moisture sensing only small θ has been used. Hence, the effect of the vegetation layer is mainly attenuation. As soil moisture increases, both the surface and the surface-volume scattering terms in (5) increase. Hence, the decrease in the surface scattering term due to layer attenuation is compensated partly by the surface-volume scattering terms.

3.0 THE FIRST-ORDER SOLUTION FOR THE PASSIVE PROBLEM

For the emission problem, the radiative transfer equations can be written in terms of the upward and downward temperatures $\bar{T}^+$, $\bar{T}^-$ and the temperature of the layer, $\bar{T}_\ell$. To account for polarization, $\bar{T}^\pm$ is taken as a column matrix

containing two elements, T_v and T_h, corresponding to vertical and horizontal polarizations. Since natural emission is incoherent the third and fourth Stokes parameters are zero. It is usual to assume that $\bar{T}^{\pm}$ are independent of the azimuth angle [10]. Thus,

$$\mu_s \frac{d\bar{T}^+}{dz} = -\bar{K}_e \bar{T}^+ + \bar{K}_a \bar{T}_\ell + \bar{F}^+ \quad , \tag{9}$$

$$\mu_s \frac{d\bar{T}^-}{dz} = \bar{K}_e \bar{T}^- - \bar{K}_a \bar{T}_\ell + \bar{F}^- \quad , \tag{10}$$

where

$$\bar{F}^{\pm} = \frac{1}{2} \int_0^1 \bar{K}_s \bar{P}(\pm\mu_s,\mu) \bar{T}^+(z,\mu)\, d\mu$$

$$+ \frac{1}{2} \int_0^1 \bar{K}_s \bar{P}(\pm\mu_s,-\mu) \bar{T}^-(z,\mu)\, d\mu \quad , \tag{11}$$

where $\bar{P}(\pm\mu_s,\mu)$ is the zeroth-order Fourier component of the phase matrix; $\bar{K}_a$ is the absorption coefficient matrix (Appendix A). The boundary condition of the ground surface is

$$\bar{T}^+(-d,\mu_s) = \frac{1}{2} \int_0^1 \bar{G}(\mu_s,\mu) \bar{T}^-(-d,\mu)\, d\mu + \bar{e}_g \bar{T}_g \quad , \tag{12}$$

where $\bar{G}$ is the zeroth-order Fourier coefficient of the surface phase matrix,

$\bar{e}_g$ is the emissivity of the ground surface, and $\bar{T}_g$ is the temperature of the ground medium. The procedure to solve (9)-(12) up to the first-order assuming small $\bar{K}_s$ is the same as in the active problem given in the previous section when we leave out step (a). The solution for $\bar{T}^+(0,\mu)$ including zeroth-order and significant terms in the first-order is

$$\bar{T}^+(0,\mu_i) = \left[\bar{1} - e^{-\bar{K}_{ei}d} + \bar{M}_2 - \bar{M}_1 - \bar{M}_3\right](1-\omega)\,\bar{T}_\ell + \left(e^{-\bar{K}_{ei}d} + \bar{M}_1\right)\left\{0.5\,\ddot{G}(\mu_i,\mu_j)\,(1-\omega)\left(1 - e^{-\bar{K}_{ei}d}\right)\bar{T}_\ell + \bar{e}_g\,\bar{T}_g\right\}, \tag{13}$$

where $\bar{1}$ is the identity matrix; ω is the albedo of the layer; μ_i, μ_j are the outgoing and incoming direction cosines corresponding to the points chosen for an N-point quadrature integration; and $e^{-\bar{K}_{ei}d}$ is the diagonal matrix,

$$e^{-\bar{K}_{ei}d} = \text{Diag}\left[e^{-K_{ev}d/\mu_1},\ldots, e^{-K_{ev}d/\mu_N}, e^{-K_{eh}d/\mu_1},\ldots, e^{-K_{eh}d/\mu_N}\right],$$

In (13), $1 \le i, j \le N$. The matrices $\bar{M}_{1,2,3}$ represent volume scattering operators and their elements denoted by $(m_{pq})_{ij}$ for a polarization component pq (p,q=v or h) are related to the elements of the phase matrix $\bar{P}$ as

$$(m_{1pq})_{ij} = 0.5\,K_{spi}\,P_{pq}(\mu_i,\mu_j)\left(e^{-K_{epi}d} - e^{-K_{eqj}d}\right)/(K_{eqj}-K_{epi}),$$

$$(m_{2pq})_{ij} = 0.5\,K_{spi}\,[P_{pq}(\mu_i,\mu_j) + P_{pq}(\mu_i,-\mu_j)]\left(1 - e^{-K_{epi}d}\right)/K_{epi},$$

$$(m_{3pq})_{ij} = 0.5\, K_{spi}\, P_{pq}(\mu_i,\mu_j) \left[1 - e^{-(K_{epi}+K_{eqj})d}\right]/(K_{epi}+K_{eqj}) \quad ,$$

where $K_{spi}=K_{sp}/\mu_i$, $K_{epi}=K_{ep}/\mu_i$, and $K_{eqj}=K_{eq}/\mu_j$. In (13) terms involving $\bar{M}$ represent the first-order corrections to the zeroth-order terms. It is interesting to note that irrespective of order the major sources of emission are the upward and downward emissions of the layer and upward emission from the ground. These source emissions can either propagate directly or be scattered by the layer boundary towards the point of observation with an appropriate amount of attenuation (zeroth-order terms). They can also be scattered by the layer inhomogeneities with or without additional scattering by boundary towards the point of observation (first-order terms). Terms which represent scattering of these emissions first downward and then upward by the ground surface have been ignored in (13).

Usually the upward emission from the layer is at least comparable to that from the ground for a fully grown vegetation cover. Hence, the ground emission term cannot dominate the total emission. The downward layer emission which is scattered upward by the ground is also sensitive to soil moisture condition. Its increase with the increase in soil moisture compensates the simultaneous decrease in ground emission. As a result the sensitivity to soil moisture can be reduced by 50% or more when the optical depth of the layer is 0.4.

4.0 SCATTERING CHARACTERISTICS OF A VEGETATION LAYER

In this section we want to show the relative contributions of the terms in (5) as a function of the incidence angle at different albedo, optical depths, and ground permittivities. For the purpose of illustration, Kirchhoff

surface model written in series form [11] and Rayleigh phase matrix [2] are used in Figs. 2-5. Fig. 2 illustrates the contributions of the three types of terms discussed in Section 2 at an optical depth of 0.1. It is seen that the surface-volume scattering term is much more important for horizontal polarization than vertical polarization at large angles of incidence. Furthermore, the horizontally polarized surface-volume scattering term also becomes comparable to the volume scattering term at large angles of incidence. This is true particularly when the ground moisture is large while optical thickness is relatively small. In this case, soil moisture sensing is possible at large angles of incidence even though the surface scattering term is small at these angles. Fig. 3 shows that for thicker optical depth the surface-volume scattering term becomes comparable to the surface scattering term at much smaller incidence angles than when the optical depth is small (Fig. 2). This implies that the surface-volume scattering term tends to reduce the loss in sensitivity to soil moisture sensing as optical depth increases. In Fig. 4 the backscattering coefficients for the three types of terms in (5) are plotted versus the optical depth at two different permittivities when the incidence angle is 8.6°. The surface-volume term is small compared with the surface term. When the same calculations are repeated at 20° incidence in Fig. 5, we see that the surface-volume scattering term becomes important and can exceed the surface scattering term if optical depth is large. Since soil moisture sensing is usually conducted between 10° to 20°, these results indicate that surface-volume scattering terms tend to reduce the loss in sensitivity of the surface scattering term when the optical depth is large ($\tau > 0.4$). To summarize these results, the ratio of the change in the backscattering coefficients between a wet (soil permittivity = 18) and a dry (soil permittivity = 3.5) soil condition, with vegetation cover present

to that with no vegetation cover is plotted in Fig. 6 using the disc phase function (Appendix A). This ratio is shown as a function of optical depth. It depicts the loss in sensitivity in sensing a vegetated soil versus a bare soil. As expected the loss in sensitivity increases with the increase in optical depth or albedo.

5.0 EMISSION CHARACTERISTICS OF A VEGETATION LAYER

The angular characteristics of emission from a wet (ϵ=25) and a dry soil (ϵ=4) surface with vegetation cover is shown in Fig. 7. Unlike surface emission, there is very little difference in angular trends between horizontal and vertical polarizations at an optical depth close to unity. Note that the zeroth-order theory [(13) without the M_1-terms] in common use is quite inadequate unless both albedo and optical thickness are very small. This point is illustrated in Fig. 8 where zeroth, first, and exact (numerical) solutions are compared.

In Fig. 7 the level of upward emission by the layer is much higher than the emissions by the soil surface at all nadir angles even for the dry soil case. At smaller optical depth (τ<0.8) (Fig. 9) surface emission may be comparable or higher than layer emission. The surface emission term is higher and the I term (downward emission scattered upward by the soil surface) is lower for the dry case than the wet case. This shows that the change in soil emission due to change in moisture is reduced by the term in general. As albedo decreases it is expected that layer emission will increase while surface emission may suffer a slight decrease.

Thus, for the same optical depth, a smaller albedo leads to a smaller difference in total emission between the wet and the dry soil conditions because the upward layer emission is larger and surface emission is somewhat

lower. In summary, the ratio of the change in emissions from a wet and a dry soil surface with vegetation cover to that from the same surface without vegetation cover is shown as a function of optical depth in Fig. 10 using the disc phase function. It is seen that a larger albedo results in a better sensitivity to soil moisture change because scattered contribution from soil surface has increased while the upward layer emission has decreased. Upon comparing Fig. 6 with Fig. 10, it is seen that, in general, vegetation causes a more severe degradation in sensitivity on passive sensing than on active sensing. It is interesting to note that while larger layer albedo helps to improve the sensitivity somewhat in passive sensing, it has a significant adverse effect on active sensing.

Summary of Layer Parameter Effects On Soil Moisture Sensing

Layer Parameters	Sensitivity Active	Sensitivity Passive
ω ↗	↘	↗
τ ↗	↘	↘

6.0 COMPARISON WITH MEASUREMENTS

The reductions in sensitivity for the active (Fig. 6) and passive (Fig. 10) sensing of soil moisture are computed from reported measurements and plotted in Figs. 6 and 10, respectively. The procedure used to generate the data points in Fig. 6 is as follows:

(a) Scattering coefficient, σ^o, measurements at 10° incidence angle, C-band, HH polarization, on bare soil, wheat, corn and soybeans are taken from [12,13,14]. σ^o measured from wheat, corn, and soybeans will be referred to as σ^o (total).

(b) Regression lines are generated for each crop and bare soil in the form of σ^o versus soil moisture. An example is shown in Fig. 11.

(c) To estimate optical depth at 10° incidence for a given crop, we plot σ^o(total) versus σ^o(bare soil) for various values of soil moisture [6]. This plot is in real numbers. Since $\sigma^o(\text{total}) \equiv [\exp(-2\tau/\cos\theta)]\ \sigma^o(\text{bare soil}) + \sigma^o(\text{crop})$, the slope of the regression line of σ^o(total) versus σ^o(bare soil) is equal to $\exp(-2\tau/\cos\theta)$. Hence, the optical depth τ can be estimated [6].

(d) Knowing the optical depth, we can use the regression lines for σ^o(total) and σ^o(bare soil) to find a value for the ratio,

$$\frac{\left[\sigma^o_{dB}(\text{wet}) - \sigma^o_{dB}(\text{dry})\right]_{\text{total}}}{\left[\sigma^o_{dB}(\text{wet}) - \sigma^o_{dB}(\text{dry})\right]_{\text{bare soil}}}$$

which is plotted as a data point on Fig. 6.

The data points in Fig. 10 are obtained from the emissivity data reported by Wang et al. [15]. The procedure is as follows:

(a) The regression lines on the emissivity data obtained by Wang et al. [15] for various vegetations versus moisture (or permittivity) are fitted by the theoretical model [(13)]. It turns out that there is no appreciable difference between the theoretical and the regression lines. Hence, each line in Fig. 12 represents both regression and theoretical lines. It is found that the slope of the regression line is sensitive to the optical depth, while the level is sensitive to albedo. Hence, each fit provides an estimate of both albedo and optical depth (Fig. 12) for a given vegetation layer.

(b) Knowing albedo and optical depth for a given vegetation layer we

can compute the ratio

$$\frac{[T(\text{wet}) - T(\text{dry})]_{\text{total}}}{[T(\text{wet}) - T(\text{dry})]_{\text{bare soil}}}$$

and plot it as a data point in Fig. 10.

7.0 CONCLUSIONS

Scattering and emission theories up to the first-order are derived and expressed in a form which permits easy identification of the zeroth- and first-order terms as well as simple interpretation of the scattering and emission processes. Upon comparing the loss in sensitivity in soil moisture sensing due to vegetation cover, it is found that the loss is less in active sensing than passive sensing. One reason is that the volume-surface scattering term contributes positively in active sensing, while the downward emission scattered upward by the ground surface contributes negatively in passive sensing. Another reason is that emission from vegetation is of the same order as that from the ground while scattering from the ground is usually much larger than that of the vegetation at small incidence angles.

ACKNOWLEDGMENTS

This work was supported by NASA Goddard Space Flight Center under Grant NAG5-268.

REFERENCES

[1] A. K. Fung and M. F. Chen, "Scattering from a Rayleigh layer with an irregular interface," Radio Science, vol. 16, no. 6, November-December 1981, pp. 1337-1347.

[2] A. K. Fung and H. J. Eom, "A theory of wave scattering from an inhomogeneous layer with an irregular interface," IEEE Trans. Ant. and Prop., vol. AP-29, no. 6, November 1981, pp. 899-910.

[3] A. K. Fung and M. F. Chen, "Emission from an inhomogeneous layer with irregular interfaces," Radio Science, vol. 16, no. 3, May-June 1981, pp. 289-298.

[4] A. K. Fung and H. J. Eom, "Emission from a Rayleigh layer with irregular boundaries," J. Quant. Spectrosc. Radiat. Transfer, vol. 26, no. 5, 1981, pp. 397-409.

[5] A. K. Fung and H. J. Eom, "Scattering from a random layer with application to snow, vegetation, and sea-ice," Accepted for publication in IEE Proceedings-F, Communications, Radar, and Signal Processing, 1983.

[6] F. T. Ulaby, A. Aslam, and M. C. Dobson, "Effects of vegetation cover on the radar sensitivity to soil moisture," IEEE Trans. Geosci. Remote Sensing, vol. GE-20, no. 4, October 1982, pp. 476-481.

[7] F. T. Ulaby, M. Razani, and M. C. Dobson, "Effects of vegetation cover on the microwave radiometric sensitivity to soil moisture," IEEE Trans. Geoscience and Remote Sensing, vol. GE-21, no. 1, January 1983, pp. 51-61.

[8] E. P. W. Attema and F. T. Ulaby, "Vegetation modeled as a water cloud," Radio Science, vol. 13, 1978, pp. 357-364.

[9] A. Ishimaru, Wave Propagation and Scattering in Random Media, Vol. 1, Academic Press, New York, 1978, p. 17.

[10] L. Tsang and J. A. Kong, "The brightness temperature of a half-space random medium with nonuniform temperature profile," Radio Science, vol. 10, 1975, pp. 1025-1033.

[11] F. T. Ulaby, R. K. Moore, and A. K. Fung, Microwave Remote Sensing: Active and Passive, Vol. 2, Addison-Wesley, Reading, Massachussetts, 1982, p. 939.

[12] C. Dobson, H. Stiles, D. Brunfeldt, T. Metzler, and S. McMeckin, "Data documentation: 1975 MAS1-8 and MAS8-18 vegetation experiments," RSL TR 264-15, Remote Sensing Laboratory, Univ. of Kansas, Lawrence, Kansas, December 1977.

[13] G. A. Bradley, "1978 agriculture soil moisture experiment (ASME) data documentation," RSL TR 460-3, Remote Sensing Laboratory, Univ. of Kansas, Lawrence, Kansas, October 1980.

[14] B. W. Milstead, "Agricultural soil moisture experiment: 1978 Colby (Kansas): Data Catalog and documentation," JSC-16229, NASA Johnson Space Center, Houston, Texas, September 1979.

[15] J. R. Wang, J. E. McMurtrey, III, E. T. Engman, T. G. Jackson, T. J. Schmugge, W. I. Gould, J. E. Fuchs, and W. S. Glazar, "Radiometric measurements over bare and vegetated fields at 1.4 GHz and 5 GHz frequencies," Remote Sensing of Environment, vol. 12, 1982, pp. 295-311.

[16] H. J. Eom and A. K. Fung, "A scatter model for vegetation up to Ku-band," Accepted for publication in Remote Sensing of Environment, 1983.

[17] M. A. Karam and A. K. Fung, "Scattering from randomly oriented circular discs with application to vegetation," Radio Science, vol. 18, no. 3, July-August 1983, pp. 557-565.

APPENDIX A: Disc Phase Function and Extinction Coefficients

The phase matrix for a dielectric thin circular disc may be written in terms of the scattering amplitude matrix $\bar{f}$ [16] given as

$$\bar{f} = [k^2 a \ell (\epsilon-1) J_1 (a q_t)/(2 q_t)] \cdot \begin{bmatrix} (\bar{\bar{A}}\cdot\hat{v})^T\cdot\hat{v}_s & (\bar{\bar{A}}\cdot\hat{h})^T\cdot\hat{v}_s \\ (\bar{\bar{A}}\cdot\hat{v})^T\cdot\hat{h}_s & (\bar{\bar{A}}\cdot\hat{h})^T\cdot\hat{h}_s \end{bmatrix} \tag{A-1}$$

where

$k = 2\pi/\lambda$: free space wave number,

a : radius of disc,

ℓ : thickness of disc,

ϵ : permittivity of disc,

J_1 : first-order Bessel function of the first kind,

$q_t = k[(\sin\theta_s\cos\phi_s - \sin\theta\cos\phi)^2 + (\sin\theta_s\sin\phi_s - \sin\theta\sin\phi)^2]$,

θ_s and θ are polar scattered and incident angles, respectively,

ϕ_s and ϕ are azimuthal scattered and incident angles, respectively,
(see Fig. 1 for geometry)

$\hat{v}$, $\hat{h}$, $\hat{v}_s$, and $\hat{h}_s$ are unit polarization vectors as shown in Fig. 1,

$\hat{h} = (-\sin\phi, \cos\phi, 0)$

$\hat{v} = (\cos\theta\cos\phi, \cos\theta\sin\phi, -\sin\theta)$

$\hat{h}_s = (-\sin\phi_s, \cos\phi_s, 0)$

$\hat{v}_s = (\cos\theta_s\cos\phi_s, \cos\theta_s\sin\phi_s, -\sin\theta_s)$

$\bar{\bar{A}}$ is a three by three matrix given as

$$\bar{\bar{A}} = \frac{1}{a_0} \begin{bmatrix} 1 & 0 & 0 \\ 0 & 1 & 0 \\ 0 & 0 & a_0/a_1 \end{bmatrix} \qquad \text{(A-2)}$$

where

$$a_0 = 1 + \frac{a^2 c}{2} (\varepsilon - 1) A_0$$

$$a_1 = 1 + \frac{a^2 c}{2} (\varepsilon - 1) A_1$$

$$A_0 = (a^2 - c^2)^{-1.5} \left\{ \frac{-c(a^2 - c^2)^{0.5}}{a^2} + \frac{\pi}{2} - \tan^{-1}\left(\frac{c^2}{a^2 - c^2} \right)^{0.5} \right\}$$

$$A_1 = 2(a^2 - c^2)^{-1.5} \left\{ \frac{(a^2 - c^2)^{0.5}}{c} - \frac{\pi}{2} + \tan^{-1}\left(\frac{c^2}{a^2 - c^2} \right)^{0.5} \right\}$$

In the above, a and c are major and minor semi-axes of an ellipsoid. Note that the symbol T in (A-1) denotes transpose of a column matrix.

From (A-1), the phase matrix $\bar{P}$ may be constructed as

$$\bar{P} = 4 \pi \bar{K}_s^{-1} n_0 \langle \bar{\sigma} \rangle$$

where $\bar{\sigma}$ is the Stokes matrix expressible in terms of $\bar{f}$ [9, p. 35] and n_0 is the number density of discs. $\langle\rangle$ denotes averaging over three modified Eulerian angles [17] which account for the orientations of a disc.

The extinction coefficient matrix K_e is given as

$$K_e = \text{diag}(K_v, K_h, K_3, K_4)$$

where

$$K_v = K_{av} + K_{sv}$$
$$K_h = K_{ah} + K_{sh}$$
$$K_3 = K_4 = 0.5(K_v + K_h)$$

The scattering coefficients K_{sv} and K_{sh} are

$$K_{sv} = n_0 \int d\Omega \, \langle |f_{vv}|^2 + |f_{hv}|^2 \rangle$$

$$K_{sh} = n_0 \int d\Omega \, \langle |f_{hh}|^2 + |f_{vh}|^2 \rangle$$

where $\int d\Omega$ denotes integration over the solid angle 4π. The absorption coefficients K_{av} and K_{ah} are [9, p. 17]

$$K_{av} = n_0 \, k \, \epsilon'' \, \pi \, a^2 \, \ell \, \langle |\bar{\bar{A}} \cdot \hat{v}_i|^2 \rangle$$

$$K_{ah} = n_0 \, k \, \epsilon'' \, \pi \, a^2 \, \ell \, \langle |\bar{\bar{A}} \cdot \hat{h}_i|^2 \rangle$$

where ϵ'' is the imaginary part of the disc permittivity ϵ.

FIGURE LEGEND

Figure 1. Geometry of the scatter and emission problem.

Figure 2. Angular behavior of backscattering coefficient of Rayleigh layer above irregular ground. (ω=0.1, τ=0.1, $k\sigma$=0.1, $k\ell$=10; where ω : layer albedo, τ : layer optical depth, σ : standard deviation of rough surface height, ℓ : correlation length of rough surface height, ε_g : ground permittivity, and T = S+I+V, where S : surface scattering term, I : surface-volume scattering term, V : volume scattering term).

Figure 3. Angular behavior of backscattering coefficient of Rayleigh layer above irregular ground. (ω=0.36, τ=0.98, $k\sigma$=0.1, $k\ell$=10; and T = S+I+V, where S : surface scattering term, I : surface-volume scattering term, V : volume scattering term).

Figure 4. The effect of optical depth on HH-polarized backscattering coefficient at the incidence angle θ=8.6°. (ω=0.3, $k\sigma$=0.5, $k\ell$=10; and T = S+I+V, where S : surface scattering term, I : surface-volume scattering term, V : volume scattering term).

Figure 5. The effect of optical depth on HH-polarized backscattering coefficient at the incidence angle θ=20°. (ω=0.3, $k\sigma$=0.5, $k\ell$=10; and T = S+I+V, where S : surface scattering term, I : surface-volume scattering term, V : volume scattering term).

Figure 6. Sensitivity reduction in backscattering due to a vegetation cover of optical depth τ. ($k\sigma$=0.5, $k\ell$=10; and Sensitivity Reduction = $[\sigma^{\circ}_{dB}(\text{wet}) - \sigma^{\circ}_{dB}(\text{dry})]_{\text{total}} / [\sigma^{\circ}_{dB}(\text{wet}) - \sigma^{\circ}_{dB}(\text{dry})]_{\text{bare soil}}$; wet ground ε=18; dry ground ε=3.5.) The disc phase function is used: disc thickness = 0.2 mm, disc permittivity = 23.4+j4.7, frequency = 4.3 GHz; case (i) radius of disc = 1.3 cm, volume fraction of discs = 0.35% (equivalent albedo = 0.3); case (ii) radius of disc = 0.75 cm, volume fraction of discs = 0.2% (equivalent albedo = 0.1).

Figure 7. Angular behavior of emission of Rayleigh layer above irregular ground. (ω=0.36, τ=0.98, ground rms slope = 0.15, ground (soil) and Rayleigh layer temperature = 290°K, and T=V+I+S, where V : layer upward emission, I: layer downward emission scattered upward by soil, S : soil emission scattered and attenuated by layer).

Figure 8. Comparisons between numerical, first-order, and zeroth-order solutions in emission for different albedo ω and optical depth τ. (The ground is assumed to be a plane. Ground and Rayleigh layer temperature = 300°K.)

Figure 9. The effect of optical depth on brightness temperature at the nadir angle θ=5.6°. (ω=0.3, and T=V+I+S, where V : layer upward emission, I : layer downward emission scattered upward by soil, S : soil emission scattered and attenuated by layer, ground and Rayleigh layer temperature = 290°K.)

Figure 10. Sensitivity reduction in emission due to a vegetation cover of optical depth τ. (ω : albedo, θ : nadir angle, ground rms slope = 0.15, Sensitivity Reduction = $[T(\text{wet}) - T(\text{dry})]_{\text{total}}/[T(\text{wet}) - T(\text{dry})]_{\text{bare soil}}$, wet ground ϵ=18, dry ground ϵ=3.5, T : horizontal polarized brightness temperature.) The disc phase function with the same parameters as in Fig. 6 is used.

Figure 11. Backscattering coefficient as a function of soil moisture content m_f for wheat field at C-band, 10° incidence angle.

Figure 12. Linear regression fit of emissivity from different vegetation as a function of soil moisture content m_v. (Albedo ω and optical depth τ are estimated by fitting the theory to a given regression fit. The ground permittivity ϵ=3.5 and 18 are assumed to correspond to the soil moisture m_v=7% and 21%, respectively.)

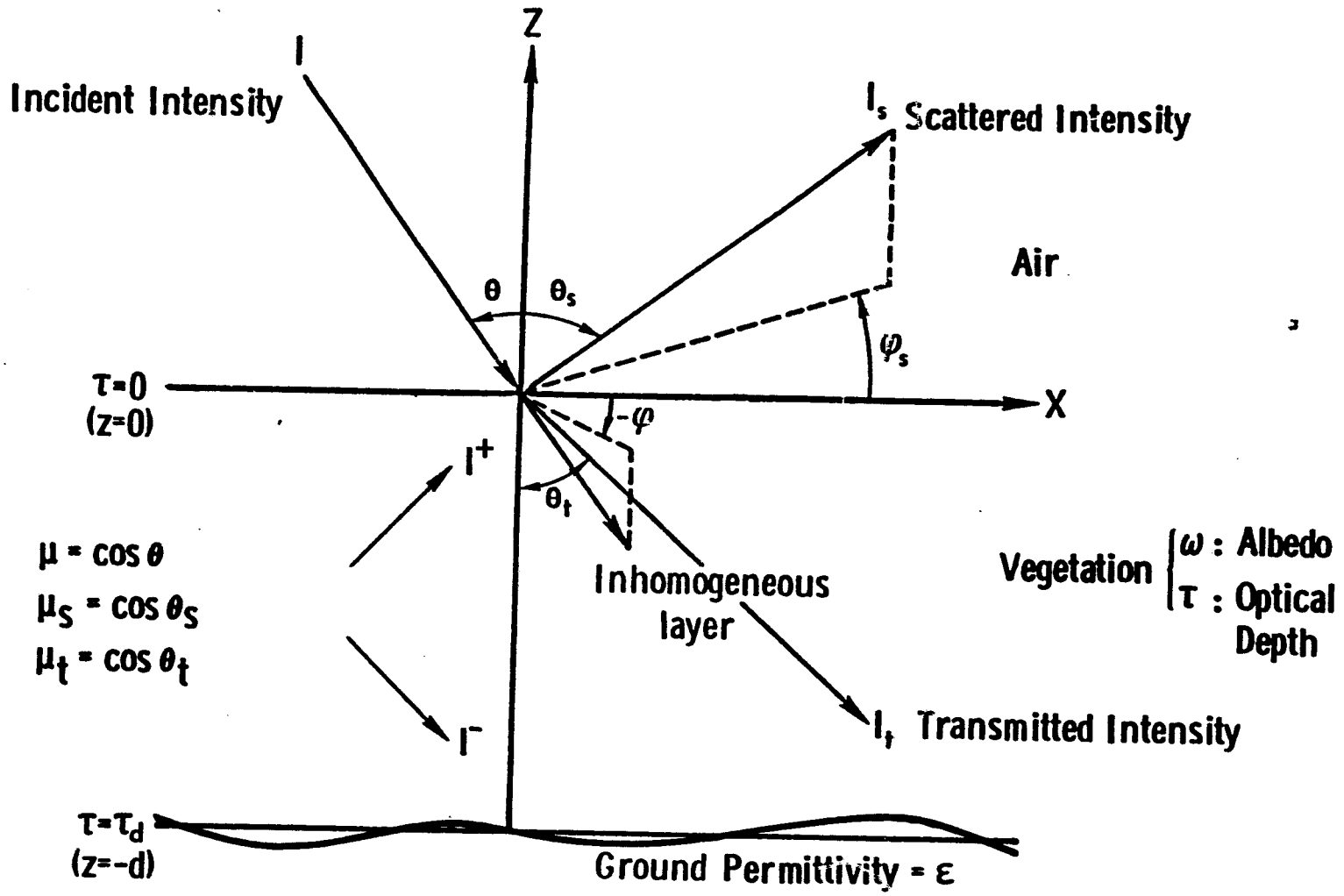
Z
I
Incident Intensity
I_s Scattered Intensity
Air
θ
θ_s
φ_s
τ=0
(z=0)
X
-φ
I^+
θ_t
$\mu = \cos\theta$
$\mu_s = \cos\theta_s$
$\mu_t = \cos\theta_t$
Vegetation
ω : Albedo
τ : Optical Depth
Inhomogeneous layer
I^-
I_t Transmitted Intensity
τ=τd
(z=-d)
Ground Permittivity = ε

Fig. 1

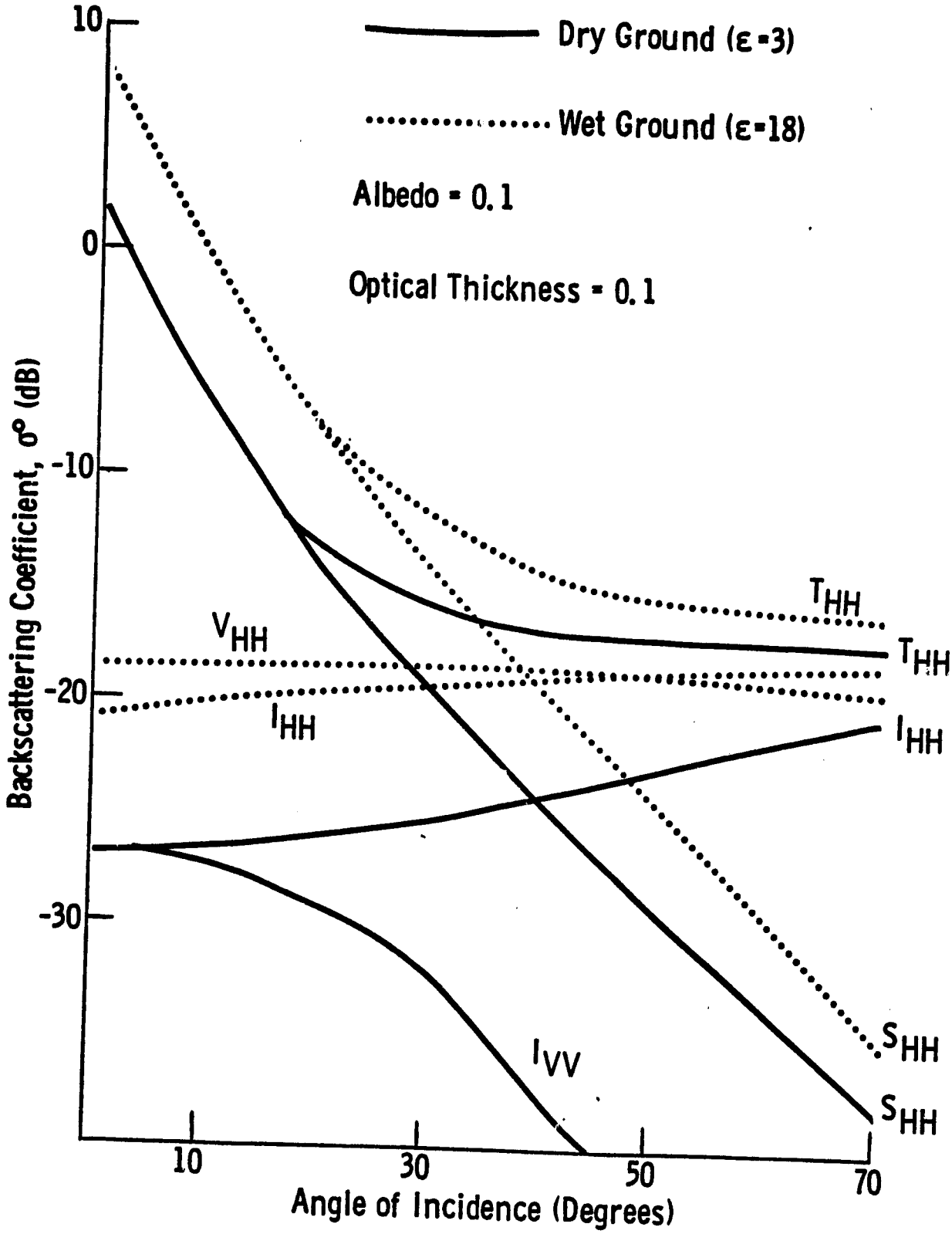
Dry Ground (ε=3)
Wet Ground (ε=18)
Albedo = 0.1
Optical Thickness = 0.1
10
0
-10
-20
-30
Backscattering Coefficient, σ° (dB)
T_{HH}
V_{HH}
I_{HH}
T_{HH}
I_{HH}
I_{VV}
S_{HH}
S_{HH}
10
30
50
70
Angle of Incidence (Degrees)

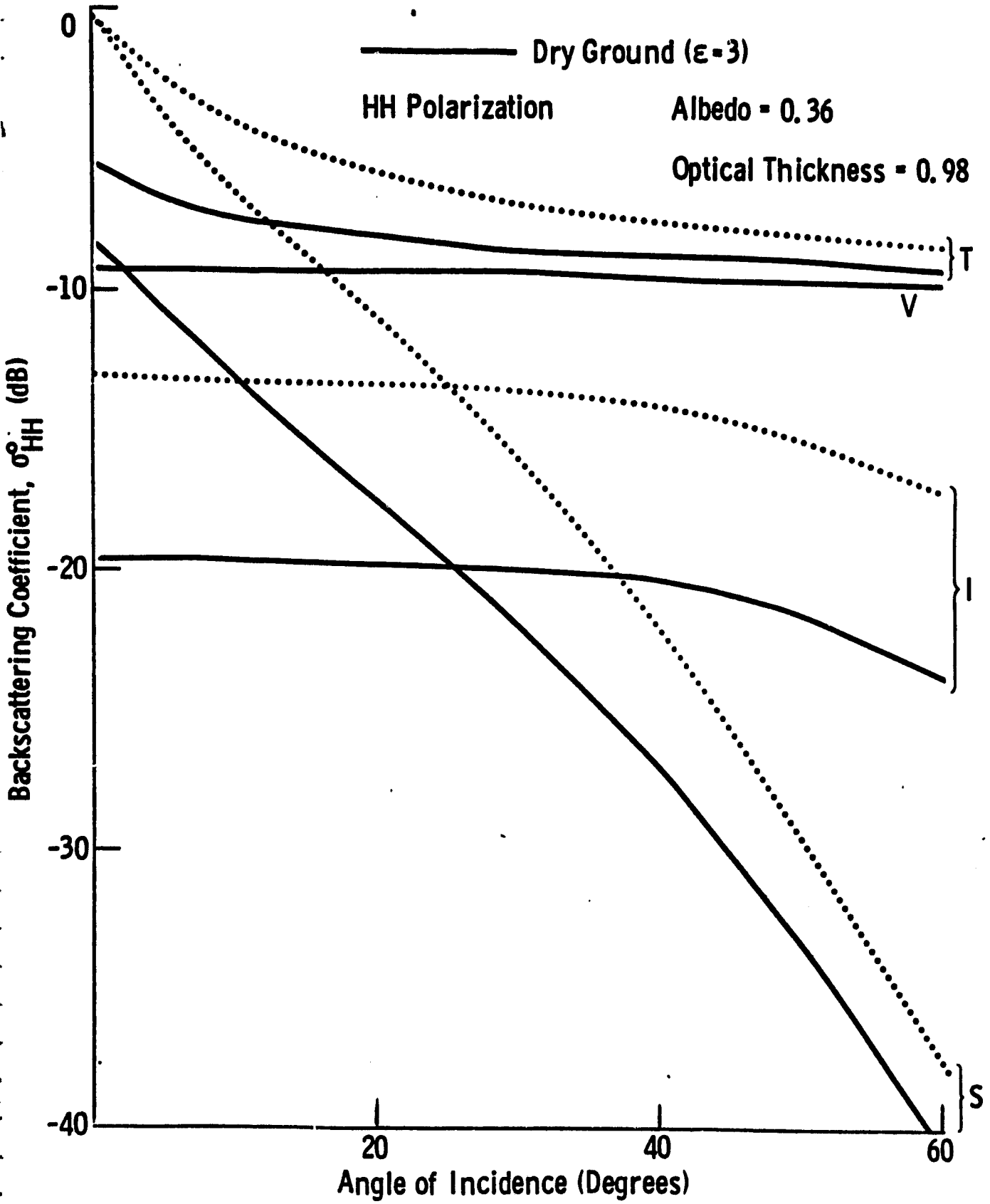
Wet Ground (ε=25)
Dry Ground (ε=3)
HH Polarization
Albedo = 0.36
Optical Thickness = 0.98
T
V
I
S
0
-10
-20
-30
-40
20
40
60
Backscattering Coefficient, σ^o_{HH} (dB)
Angle of Incidence (Degrees)

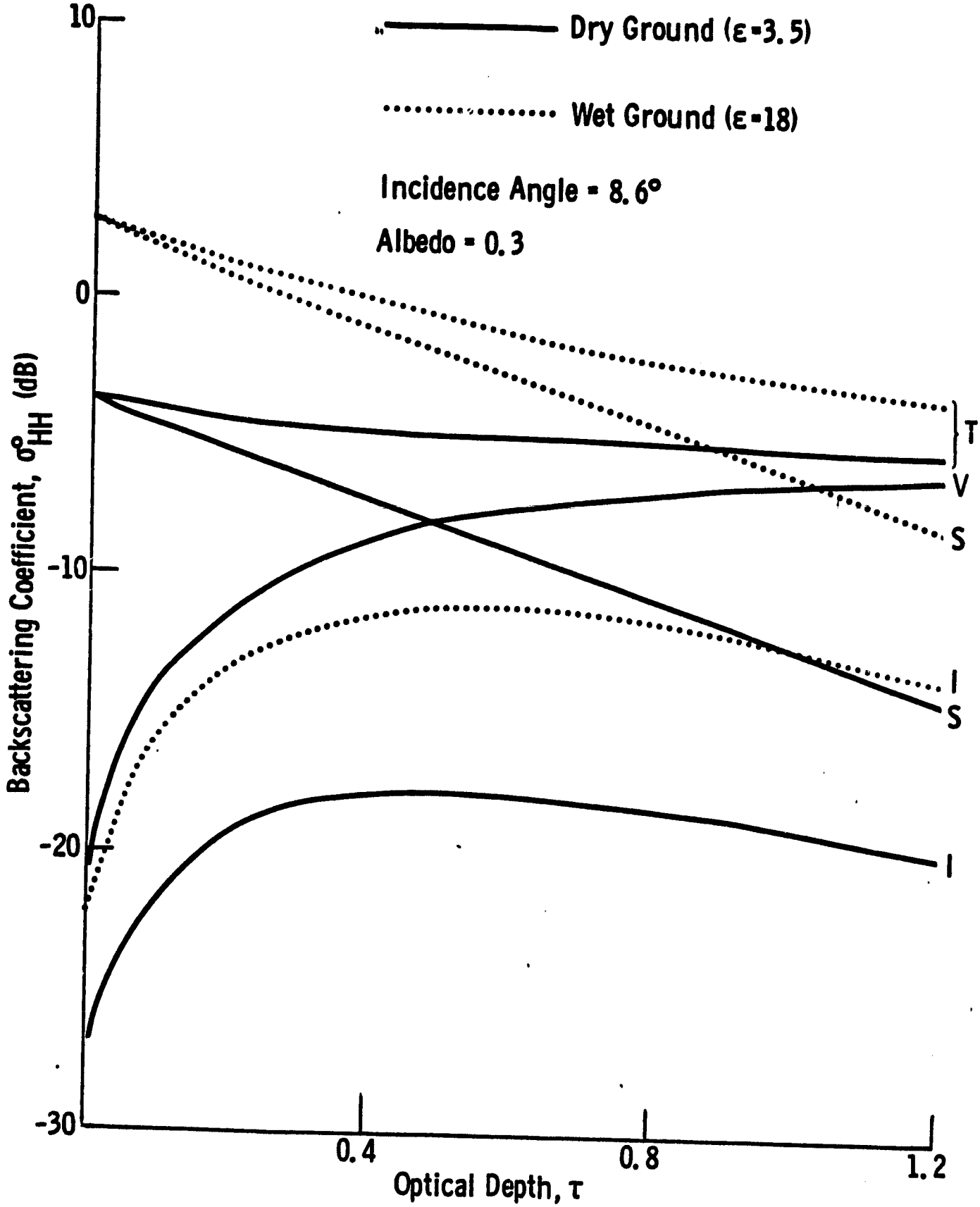
Dry Ground (ε=3.5)
Wet Ground (ε=18)
Incidence Angle = 8.6°
Albedo = 0.3
10
0
-10
-20
-30
Backscattering Coefficient, σ^{o}_{HH} (dB)
T
V
S
I
S
I
0.4
0.8
1.2
Optical Depth, τ

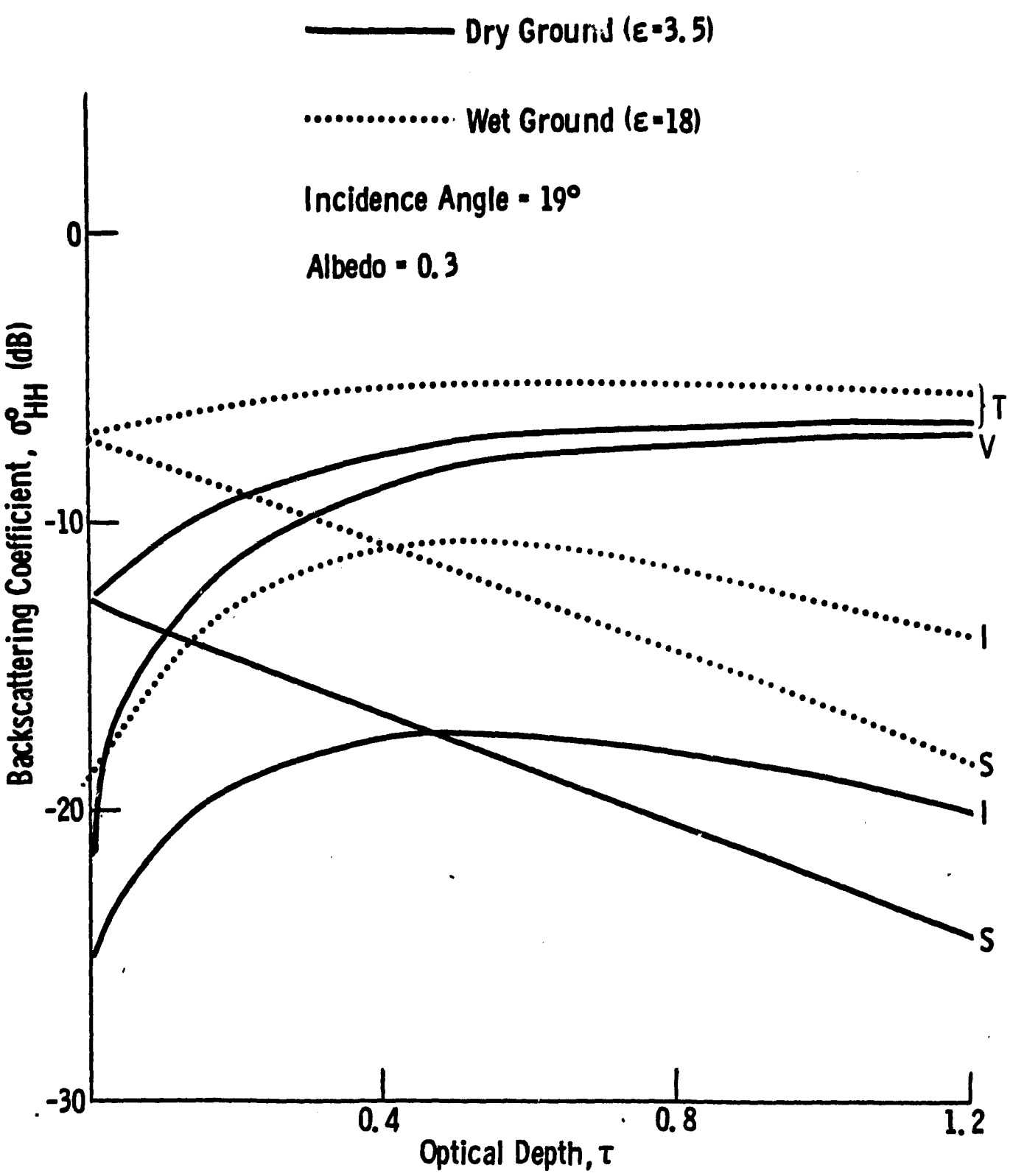
Dry Ground (ε=3.5)
Wet Ground (ε=18)
Incidence Angle = 19°
Albedo = 0.3
0
-10
-20
-30
Backscattering Coefficient, σ^o_{HH} (dB)
T
V
I
S
I
S
0.4
0.8
1.2
Optical Depth, τ

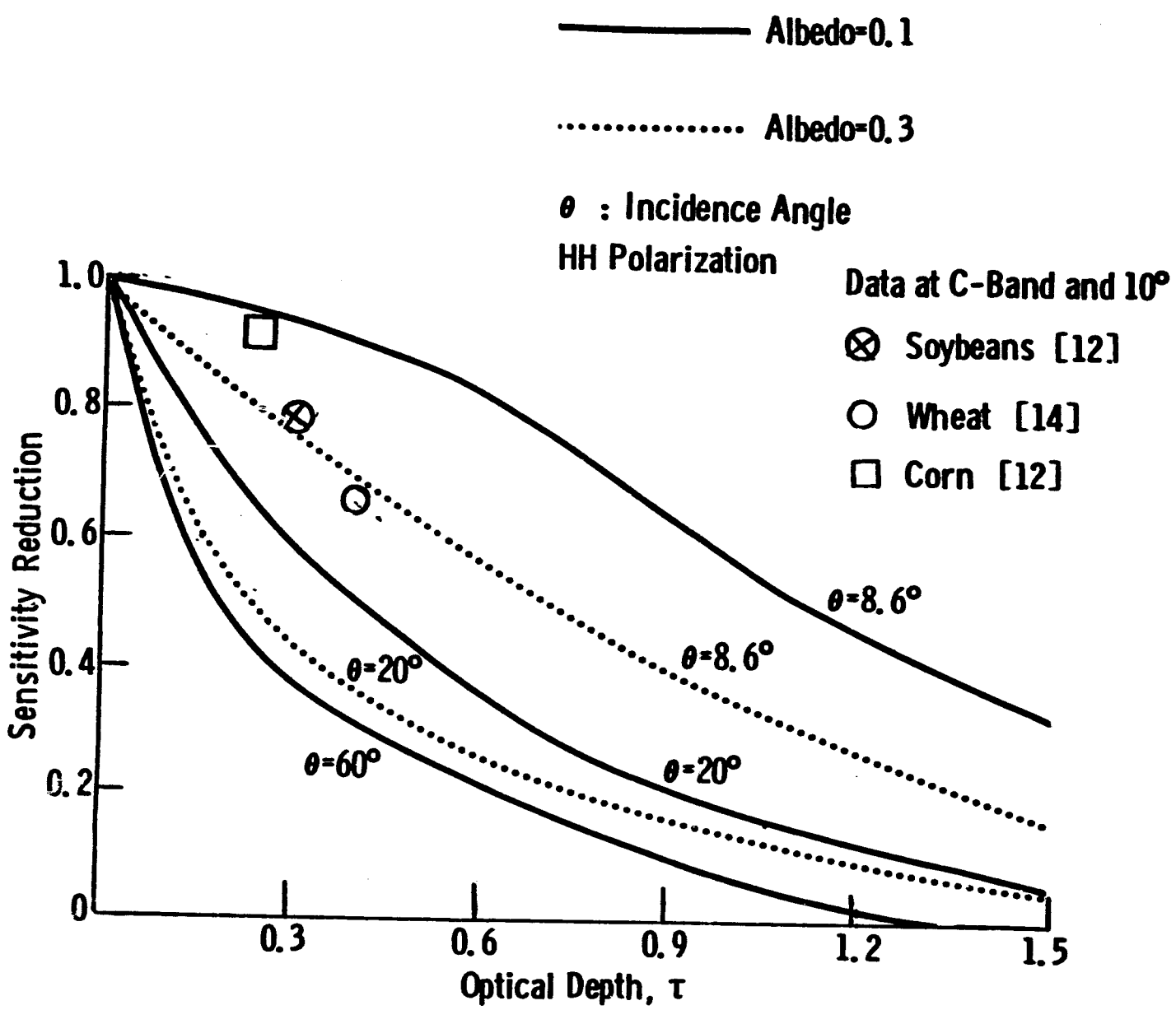
Albedo=0.1
Albedo=0.3
θ : Incidence Angle
HH Polarization
Data at C-Band and 10°
Soybeans [12]
Wheat [14]
Corn [12]
θ=8.6°
θ=8.6°
θ=20°
θ=20°
θ=60°
Sensitivity Reduction
1.0
0.8
0.6
0.4
0.2
0
0.3
0.6
0.9
1.2
1.5
Optical Depth, τ

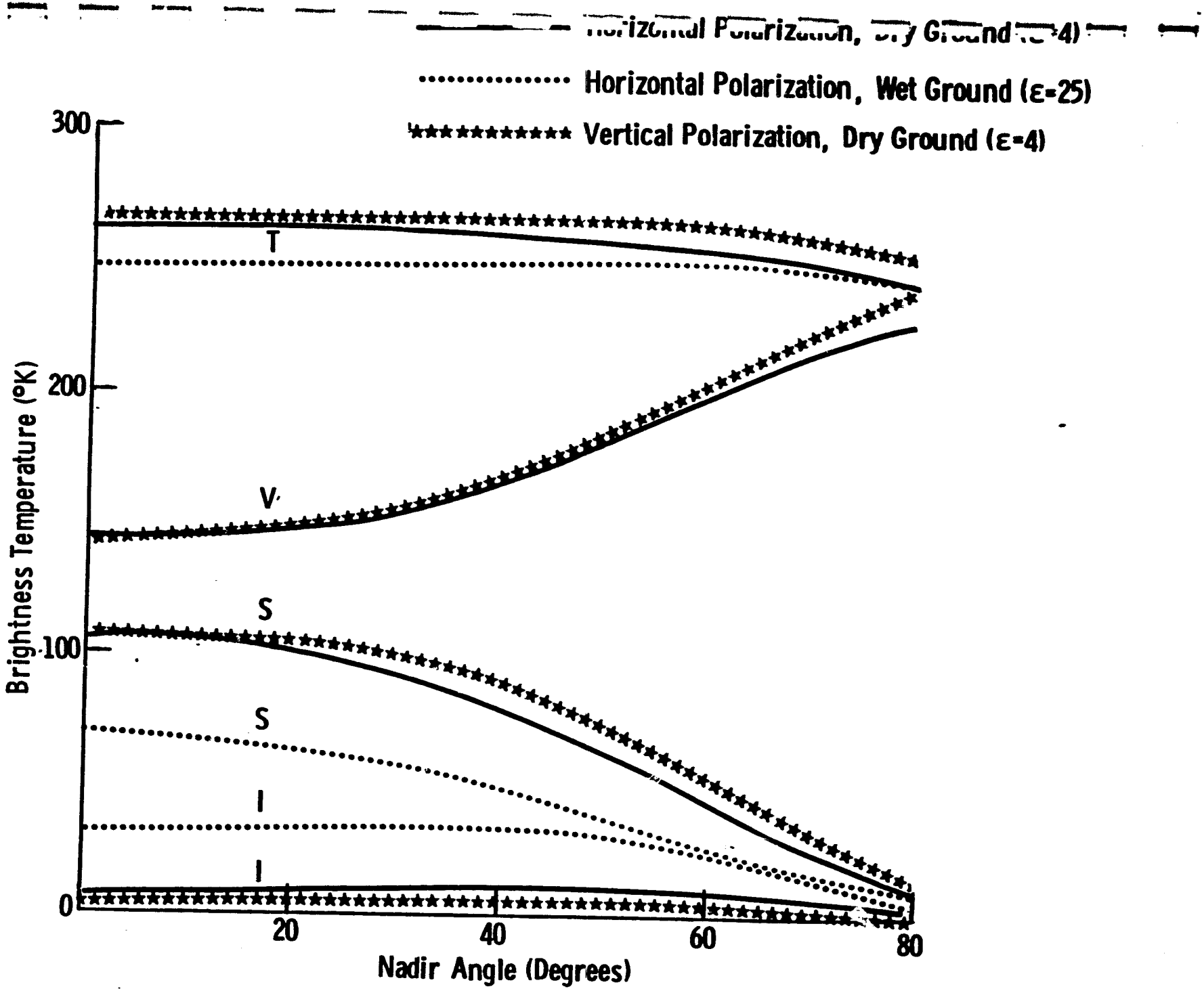
Horizontal Polarization, Dry Ground (ε=4)
Horizontal Polarization, Wet Ground (ε=25)
Vertical Polarization, Dry Ground (ε=4)
300
200
100
0
Brightness Temperature (°K)
T
V
S
S
I
I
20
40
60
80
Nadir Angle (Degrees)

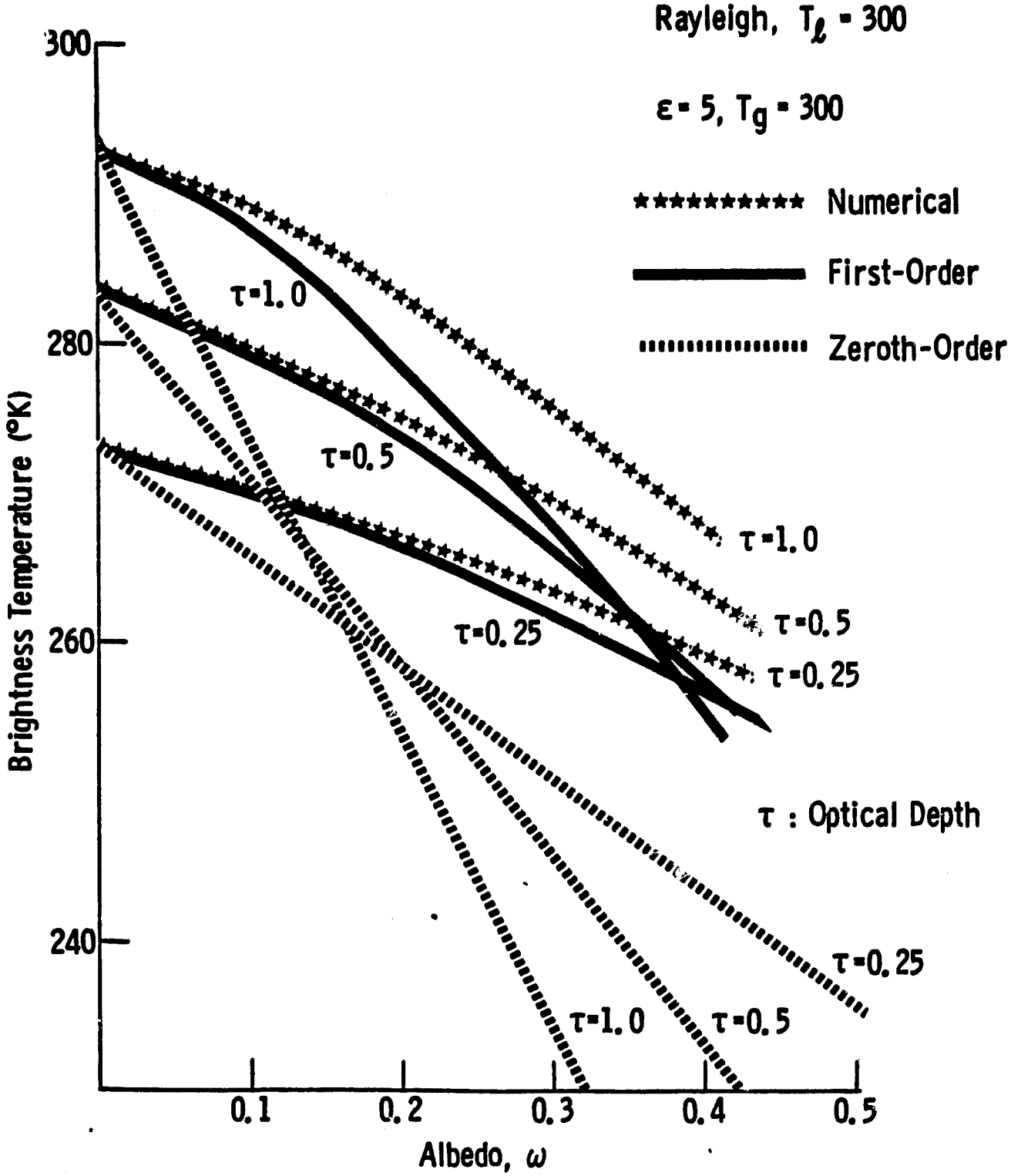
Rayleigh, T_ℓ = 300
ε = 5, T_g = 300
Numerical
First-Order
Zeroth-Order
τ=1.0
τ=0.5
τ=0.25
τ=1.0
τ=0.5
τ=0.25
τ=0.25
τ=1.0
τ=0.5
τ : Optical Depth
300
280
260
240
Brightness Temperature (°K)
0.1
0.2
0.3
0.4
0.5
Albedo, ω

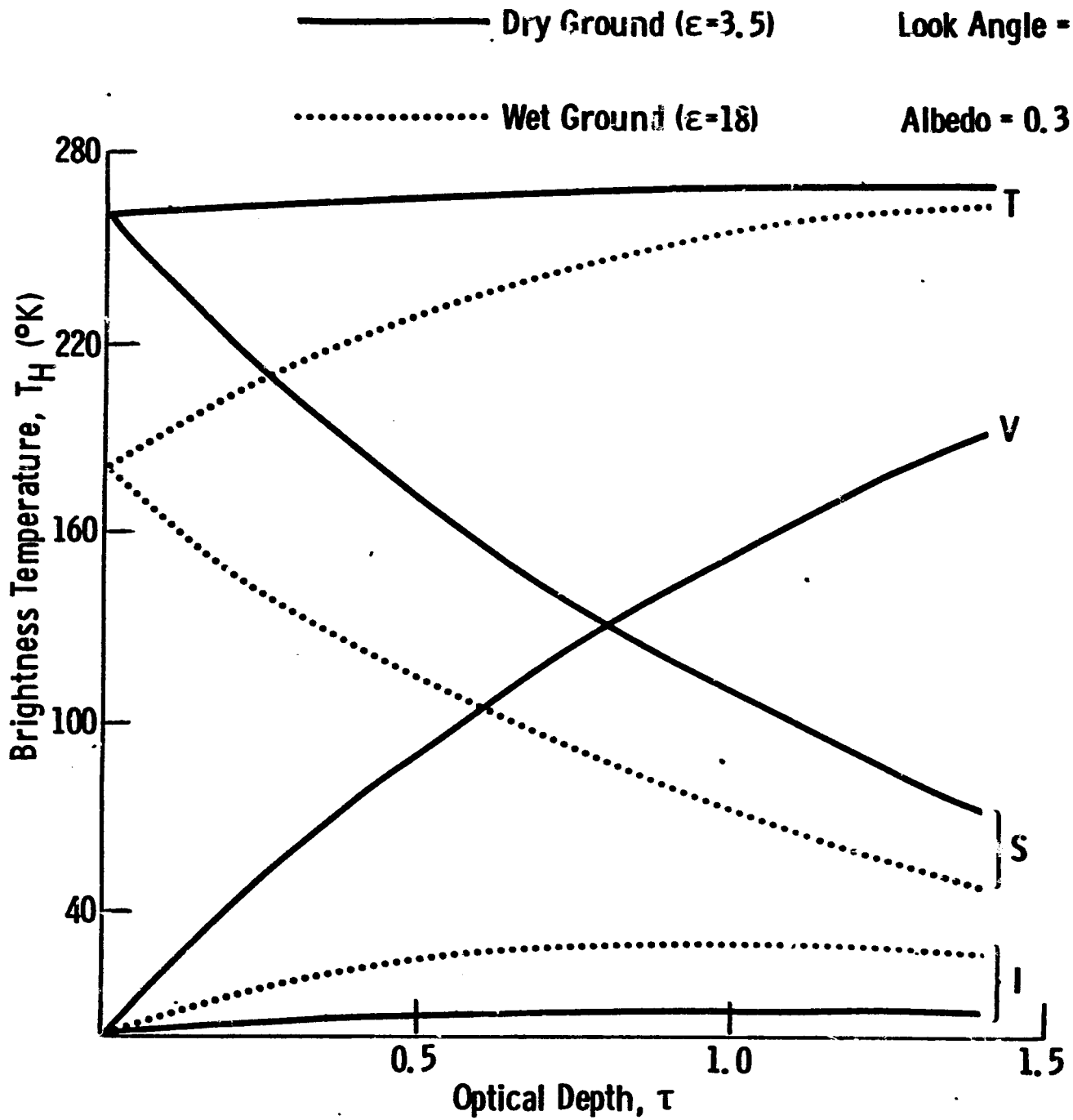
Dry Ground (ε=3.5)
Look Angle = 5.6°
Wet Ground (ε=18)
Albedo = 0.3
280
220
160
100
40
Brightness Temperature, T_H (°K)
T
V
S
I
0.5
1.0
1.5
Optical Depth, τ

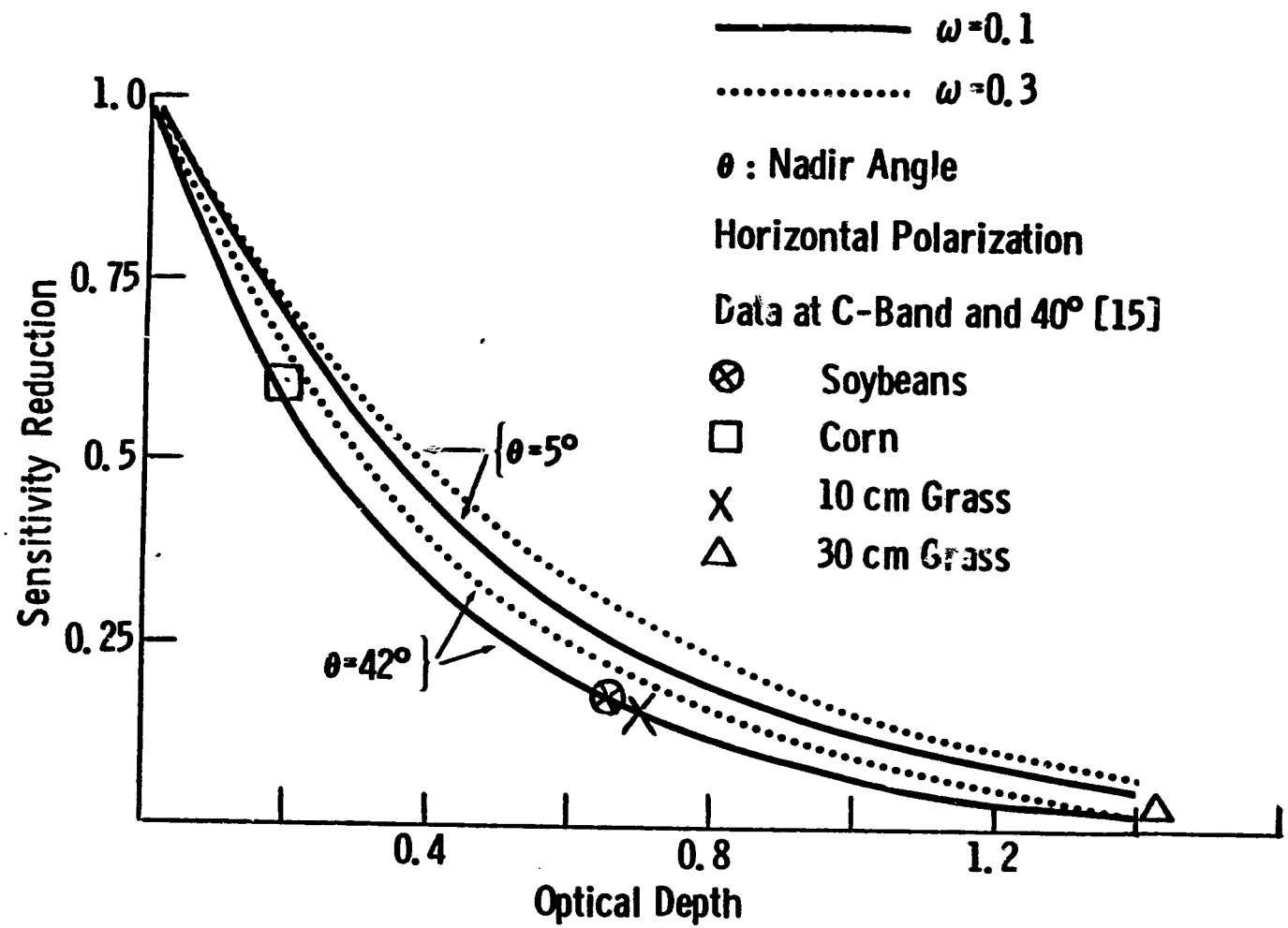
ω=0.1
ω=0.3
θ : Nadir Angle
Horizontal Polarization
Data at C-Band and 40° [15]
Soybeans
Corn
10 cm Grass
30 cm Grass
θ=5°
θ=42°
Sensitivity Reduction
1.0
0.75
0.5
0.25
0.4
0.8
1.2
Optical Depth

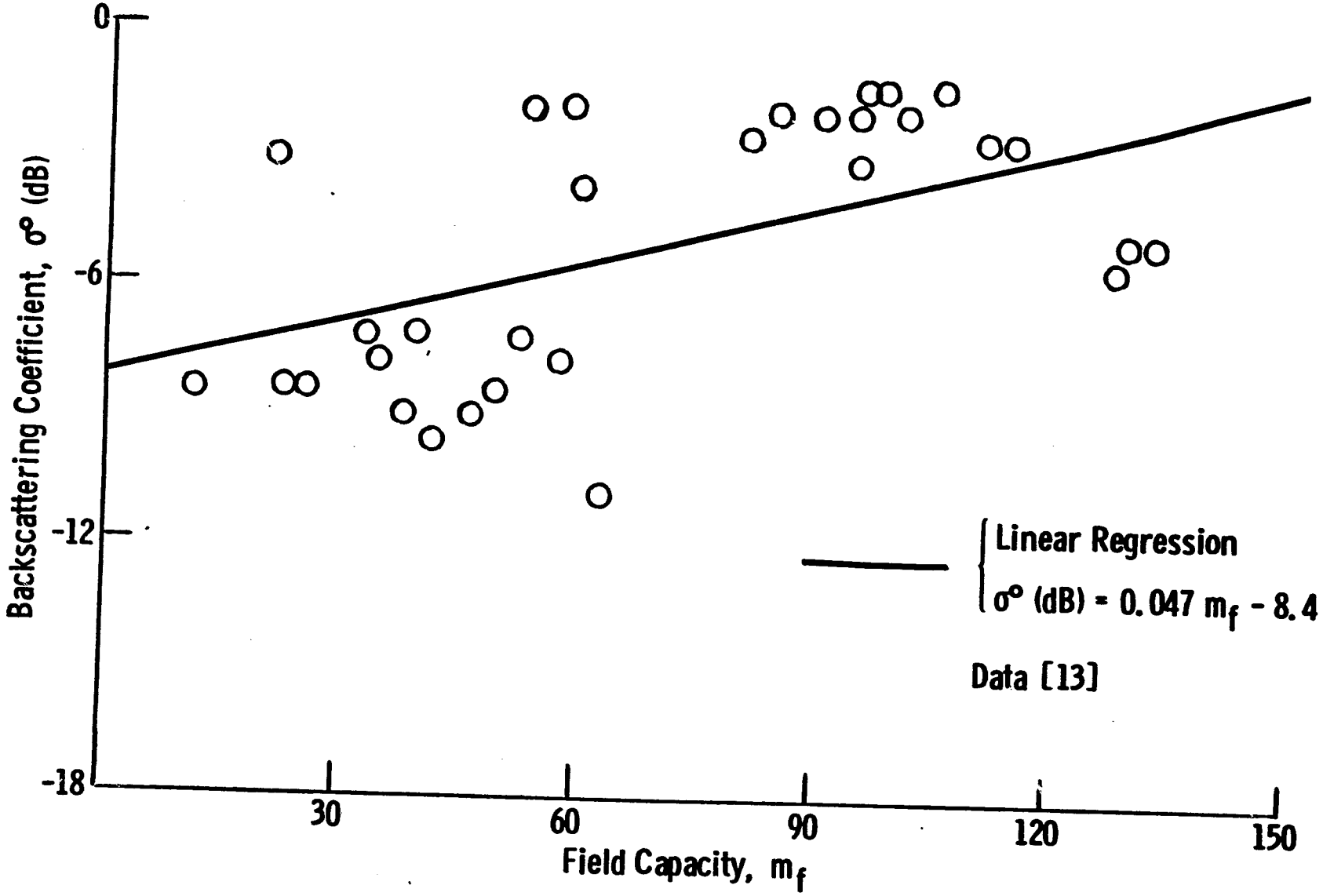
0
-6
-12
-18
Backscattering Coefficient, σ° (dB)
30
60
90
120
150
Field Capacity, m_f
Linear Regression
σ° (dB) = 0.047 m_f - 8.4
Data [13]

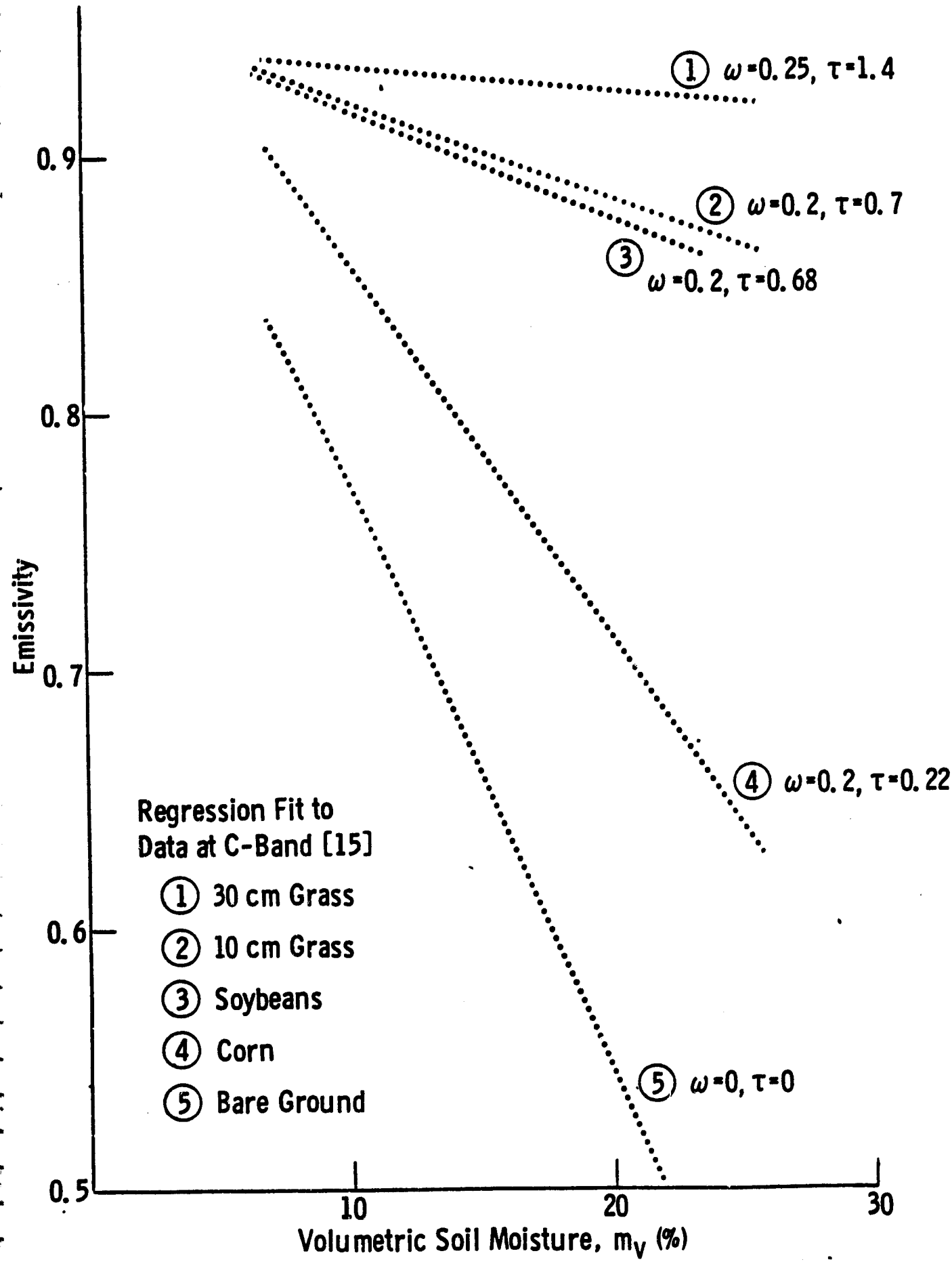
① ω=0.25, τ=1.4
② ω=0.2, τ=0.7
③ ω=0.2, τ=0.68
④ ω=0.2, τ=0.22
⑤ ω=0, τ=0
Regression Fit to
Data at C-Band [15]
① 30 cm Grass
② 10 cm Grass
③ Soybeans
④ Corn
⑤ Bare Ground
Emissivity
0.9
0.8
0.7
0.6
0.5
10
20
30
Volumetric Soil Moisture, m_v (%)